Evidence for Decreased Biological Carbon Pump Efficiency and Persistence of Photosymbiont Associations from Planktic Foraminifera across the Paleocene-Eocene Thermal Maximum

Author:
Magali Siri

Supervisors:
Prof. J.C. Zachos
Prof. A. Sluijs

May 31st 2024

Department of Earth Sciences, Utrecht University, The Netherlands
Department of Earth and Planetary Sciences, University of California, Santa Cruz, USA

ABSTRACT

The Paleocene-Eocene Thermal Maximum (PETM; ~56 million years ago) serves as an important analogue to the effects of rapid climate warming and carbon cycle perturbations. The key component to the global carbon cycle is the marine biological carbon pump (i.e., export production). The efficiency of which is dependent on the balance between the rate of organic carbon production and remineralization. Sustained surface ocean warming is expected to disrupt export production by reduced vertical mixing (stratification) and increasing rates of organic matter remineralization. Consequently, the flux of organic carbon through the water column is expected to decline, reducing the ocean's capacity to efficiently sequester carbon and altering the structure of upper ocean ecosystems (e.g., depth stratification). Assessing changes in the efficiency of the biological carbon pump, and ocean and ecosystem structure over warming periods such as the PETM is of great importance given current global warming concerns.

Here, I present novel high-resolution size-specific stable carbon and oxygen isotope records of planktic foraminifera from the South Atlantic (ODPS Site 1263, Walvis Ridge), spanning the PETM. Data from photosymbiont-bearing surface-dwelling (*Acarinina* and *Morozovella*) and asymbiotic thermocline-dwelling (*Subbotina)* planktic foraminifera is generated for the reconstruction of changes in the efficiency of the marine biological carbon pump across the PETM by evaluating surface-to-thermocline and size-dependent carbon and oxygen isotopic gradients.

The data reveal a decrease in the surface-to-thermocline $\delta^{13}C$- and $\delta^{18}O$-gradients during the CIE, suggesting a reduced efficiency of the biological carbon pump due to the shallower and more efficient remineralization of organic matter in the surface ocean. These findings support the hypothesis that PETM warming invoked a temperature-dependent increase in metabolic activity and remineralization rates in the mixed layer, which along with the effects of increased stratification resulted in decreased rates of export production in the open ocean. These findings are further supported by comparison of the $\delta^{13}C$- and $\delta^{18}O$-size covariance prior to and during the PETM, which reveals a possible inhabitance of shallower depths by *Subbotina* and narrow mixed-layer depth habitat for *Acarinina* and *Morozovella*, consistent with a shallower and more intense remineralization and reduced rated of food supply to the twilight zone.

This thesis offers new insights into the importance and resilience of photosymbiont associations in symbiont-bearing planktic foraminifera to PETM warming and environmental perturbations, contrasting the opposing theory of symbiont bleaching or loss during the PETM at ODP 1263. Instead, it is proposed that twilight zone-dwelling taxa are subjected to high stress due to deoxygenation, reduced nutrient supply, and changing upper ocean ecosystem structure during extreme warming episodes such as the PETM, to which future adaptability is hard to predict. The rate of modern climate change exceeds that of the PETM by an order of magnitude, potentially leading to drastic changes in carbon pump efficiency and biological activity far beyond the scope of PETM perturbations.

Contents

CHAPTER 1: INTRODUCTION

The ocean plays a fundamental role in maintaining life and regulating Earth's climate, as it acts as a primary reservoir for absorbing and storing heat and sequesters over a third of anthropogenic carbon from the atmosphere (Gruber et al., 2019), thereby mitigating surface warming. This absorption of carbon dioxide in the marine environment is manifested as a reduction in pH (i.e., ocean acidification), and has led to an increase in oxygen depletion in various coastal and upwelling regions (Zhang et al., 2010). The ocean's biological carbon pump (BCP) transfers carbon from the surface ocean to the deep ocean, at a mean global carbon export rate of 10.2 Pg C yr^{-1} (Nowicki et al., 2022). The past few decades, the sequestration flux of carbon has been increasing along continental margins due to increased eutrophication (Bindoff et al., 2019). However, modern carbon emissions have warmed and stratified the oceans at an unprecedented rate and by the end of the 21st century the, the open ocean is likely to significantly reduce its carbon sequestration, especially under the high-emissions RCP8.5 scenario, which forecasts a 9-16 % decrease in the global carbon settling flux (Bindoff et al., 2019). The confidence surrounding these projections are restricted by model uncertainties stemming from the complexity of the biological carbon pump.

It is important that we understand how sustained warming and extreme carbon emissions will affect the ocean's capacity to sequester atmospheric carbon, and how resilient ecosystem structures will be in the face of ongoing anthropogenic warming. By examining past warming intervals from the geological record, we can observe the ecological and environmental effects of global warming and elucidate its repercussions on short- and long-term timescales.

This research will focus on one such paleoclimate analog, the Paleocene-Eocene Thermal Maximum, and use microfossil evidence from both deep and shallow-marine environments to compile a high-resolution record of foraminiferal ecological response to global warming, in order to infer the efficiency response of the marine biological carbon pump to rapid and sustained global warming.

The remainder of this chapter will be dedicated to firstly, a general introduction to the PETM, secondly, an introduction to the biological carbon pump and perturbations in the marine biological carbon cycle during the PETM, and lastly an introduction to the physiological response of planktonic foraminifera to warming intervals. Closing this chapter will be a summary of the aims of this research, and the research questions that will be addressed.

1.1. The Paleocene-Eocene Thermal Maximum

The Paleocene-Eocene Thermal Maximum (PETM) (56.01 ± 0.05, Zeebe & Lourens, 2019) is known as the largest pre-Anthropocene warming event of the Cenozoic (Zachos et al., 2001). The PETM is globally recognized by a rapid 2–6‰ decrease in the stable carbon isotope composition ($\delta^{13}C$) of organic and inorganic compounds in both terrestrial and marine records (Bowen et al., 2004; Dickens et al., 1995, 1997; Frieling et al., 2019; John et al., 2008a; Kennett & Stott, 1991; Koch et al., 1992; McCarren et al., 2008; McInerney & Wing, 2011; Schoon et al., 2015). This signal signifies a rapid and

extreme injection of ^{13}C-depleted carbon into the global exogenic carbon pool. The coeval decrease of 1–2.5‰ in the oxygen isotope composition ($\delta^{18}O$) of biogenic calcite (e.g., John et al., 2008; Makarova et al., 2017; Zachos et al., 2006) combined with biomarker evidence (e.g., Frieling et al., 2017; Schoon et al., 2015; Sluijs et al., 2006; Sluijs, Brinkhuis, et al., 2007; Sluijs et al., 2011) and records of poleward migrations of planktonic species (e.g., Barrett et al., 2023; Crouch et al., 2001; Frieling et al., 2018; Sluijs, Bowen, et al., 2007) indicates a synchronous rapid warming of the global climate system during the PETM. Synchronously to the carbon isotope excursion (CIE), a sharp decrease in calcium carbonate ($CaCO_3$) content in deep ocean sediments implies the widespread dissolution of carbonates through deep ocean acidification (Colosimo et al., 2005; Dickens et al., 1997; Thomas & Shackleton, 1996; Zachos et al., 2005). The boron isotope ($\delta^{11}B$) and boron/calcium ratios (B/Ca) of planktic foraminifera shells suggests a sea surface pH decline of ~0.3 pH units across the PETM (Babila et al., 2016, 2018; Gutjahr et al., 2017; Penman et al., 2014).

Mean sea surface temperatures are estimated to have increased by 5.3 °C (Frieling et al., 2017). The pattern of climate warming is not spread uniformly across the globe. Data assimilations show that tropical mean SSTs increased by ~3 °C, while mid-to-high latitude SSTs warmed by 5 to 8 °C, implying amplified warming in extratropical regions (Frieling et al., 2017; Sluijs et al., 2006, 2011; Zachos et al., 2003, 2006). Estimations of equatorial sea surface warming indicates temperatures above 36 °C during the PETM (Frieling et al., 2017). Bottom-water temperatures are estimated to have warmed 4-5 °C (Thomas & Shackleton, 1996; Tripati & Elderfield, 2005; Zachos et al., 2003). Estimates of global mean surface air temperatures record an increase of 5.6 °C to a mean surface temperature of 34.2 °C, resulting in an estimated climate sensitivity of 6.5 °C (Tierney et al., 2022). This climate sensitivity is much higher than modern sensitivity estimates, indicating that climate sensitivity increases dramatically with higher greenhouse gas emissions .

The CIE is also marked by rapid turnover in floral and faunal assemblages (Gibbs, Bown, et al., 2006; Nwojiji et al., 2023; Scheibner et al., 2005; Speijer et al., 2012; Widlansky et al., 2022; Wing et al., 2005). The onset of the PETM is estimated to have lasted only 4-6 kyr (Li et al., 2022; Zeebe et al., 2016), while the complete event is estimated to have prevailed for 150-250 kyr, measured from the onset to full recovery (Murphy et al., 2010; Röhl et al., 2007; Zeebe & Lourens, 2019). Estimates of the total amount of carbon injected into the climate system during the onset range from 2,000 Gt C to over 13,000 Gt C (Cui et al., 2011; Dickens et al., 1995; Gutjahr et al., 2017; Kirtland Turner & Ridgwell, 2016; Penman et al., 2014; Zachos et al., 2005; Zeebe et al., 2009, 2016). Putting the rate of carbon emissions at the onset of the PETM at around 0.6-1.2 Pg C yr^{-1} (Li et al., 2022; Zeebe et al., 2016). Which is a magnitude lower than the annual anthropogenic emissions of the last decade, which range around 10.9 ± 0.9 Pg C yr^{-1} (2010-2019) (Canadell et al., 2021).

The primary source for the large-scale injection of ^{13}C-depleted carbon into the global exogenic carbon pool, causing the distinct CIE associated with the PETM, is not entirely known. However, most

evidence points towards the thermal dissociation of ^{13}C-depleted (–60‰) methane hydrates to have been the primary source. The release and oxidation of 1500 Pg of methane hydrates is sufficient to account for a carbon isotope excursion of –2 to –3‰ (Dickens et al., 1995), but insufficient to explain PETM warming. Astrochronological analysis and modeling suggest a possible astronomical trigger for the warming associated with the PETM, as the onset occurred close to a minimum in precession and maxima in both the 100-kyr and 405-kyr eccentricity cycles (Li et al., 2022; Piedrahita et al., 2022; Zeebe & Lourens, 2019). This orbital configuration may have induced a pre-excursion warming, acting as a trigger to positive carbon cycle feedback mechanisms such as methane hydrate dissociation (Lourens et al., 2005; Sluijs, Brinkhuis, et al., 2007; D. J. Thomas et al., 2002), or carbon release through permafrost thawing (DeConto et al., 2012; Li et al., 2022). Other proposed potential C sources include the rapid thermal combustion, decomposition and/or oxidation of terrestrial organic carbon, possibly in response to increased aridity and permafrost thawing (DeConto et al., 2012; Kurtz et al., 2003), the release of methane and CO_2 from hydrothermal vent systems associated with Large Igneous Provinces (LIPs) (Berndt et al., 2023; Frieling et al., 2016; Svensen et al., 2004), and/or the degassing of CO_2 associated with the volcanic outgassing and emplacement of flood basalt and sills associated with the North Atlantic Igneous Province (NAIP) (Gutjahr et al., 2017; Kender et al., 2021; Storey et al., 2007; Svensen et al., 2004, 2010; Wieczorek et al., 2013).

Foraminiferal carbon isotope records and ocean modelling suggest an abrupt shift in deep-ocean circulation during the PETM, with a posited shift from a Southern Hemisphere to Northern Hemisphere overturning circulation at the start of the Paleocene-Eocene Thermal Maximum (Bice & Marotzke, 2002; Lunt et al., 2010; Nunes & Norris, 2006). Although the exact shift in the location of deep-water formation remains controversial (Zeebe & Zachos, 2007), the changes in circulation supplied warm, salty intermediate waters to the equatorial and South Atlantic (Bice & Marotzke, 2002; Jennions et al., 2015; Lunt et al., 2010; Thomas et al., 2018), which may have resulted in the enhanced remineralization of organic matter in the water column. Subsequently, it may have reduced the food supply to the benthos and driving the temporary loss in benthic biodiversity and abundance (Jennions et al., 2015; Thomas et al., 2018).

Terrestrial and marine records document a substantial perturbation in the hydrological cycle during the PETM. Evidence for increased continental weathering and runoff has been recorded in sedimentological, palynological and biomarker records from the tropics (e.g., Handley et al., 2012), subtropics (e.g., Schmitz & Pujalte, 2007) and high-latitudes (e.g., Kelly et al., 2005; Pagani et al., 2006). This increase in continental weathering and runoff is generally attributed to increased seasonality, with elevated precipitation at high-latitudes and an increased frequency of extreme rainfall and flood events (Carmichael et al., 2017; Pagani et al., 2006; Schmitz & Pujalte, 2007).

Recovery from the PETM carbon cycle perturbations was on the order of 30-40 kyr (Bowen & Zachos, 2010; Murphy et al., 2010). This rapid recovery required efficient carbon sequestration

mechanisms to draw down the extremely high atmospheric CO_2-levels. The most efficient and likely mechanism for rapidly removing carbon from the atmosphere is the enhanced weathering of silicates (Brault et al., 2017; Kelly et al., 2005; Penman, 2016; Zachos et al., 2005), however, this alone may not have been sufficient to account for the rapidity of the CIE recovery (Bowen & Zachos, 2010). Carbon sequestration through the marine biological carbon pump (BCP) provides another pathway for drawing down atmospheric carbon and aiding in the recovery of the CIE, particularly along continental margins (Papadomanolaki et al., 2022). However, the integrated effects of higher temperatures, elevated pCO_2-levels, ocean acidification, and the differential changes in ocean circulation and the hydrological cycle create an entirely enigmatic scenario for PETM ocean productivity, export production and subsequently the biological carbon pump (Ma et al., 2014).

1.2. The Marine Biological Carbon Pump

The marine biological carbon pump (BCP) plays a crucial role in transferring carbon from the atmosphere and surface ocean to the ocean interior and seafloor sediments over geological timescales (Fig. 1). The efficiency of the biological carbon pump is regulated by the rate of photosynthetic organic matter formation and its degradation through microbial respiration/remineralization through the water column. The balance between these processes may be traced through the exponential decrease in $\delta^{13}C_{DIC}$ with depth, the resulting $\delta^{13}C_{DIC}$-gradient which serves as a good proxy for the efficiency of the biological carbon pump.

Changes in surface ocean productivity can directly affect export fluxes and atmospheric CO_2-levels on geological timescales by acting as either a positive or negative feedback mechanism on the climate system, depending on the direction of change. Increased productivity is suggested to aid in the drawdown of atmospheric CO2-levels and act as a buffer against the development of a greenhouse climate, while the opposite holds true in the case of decreased productivity. However, even if productivity remains unchanged, the efficiency of the biological pump at sequestering carbon into the deep ocean may still be compromised by the effects of warming, ocean acidification, and changes in the structure of the water column (i.e., stratification) and ecosystem structure.

Rising temperatures and ocean acidification reduce the efficiency of the carbon pump at taking up atmospheric carbon and transferring it to the interior and deep ocean. The combined effects of ocean warming, and increased carbonate dissolution hamper the formation of biogenic $CaCO_3$. As a result, aggregate ballasting and settling rates are reduced, leading to prolonged exposure of organic matter to remineralization in the twilight zone, subsequently limiting the amount of organic matter reaching the ocean floor (Mendes & Thomsen, 2012). Additionally, metabolic theory suggests that metabolic rates –which control the rates of organic matter formation through photosynthesis and its microbial degradation through remineralization – are sensitive to changes in ocean temperature (Allen et al., 2005; Cossins & Bowler, 1987), and subsequently affect BCP efficiency and pCO_2-levels on geological timescales (Boscolo-Galazzo et al., 2018). At times of global warming, increased metabolic

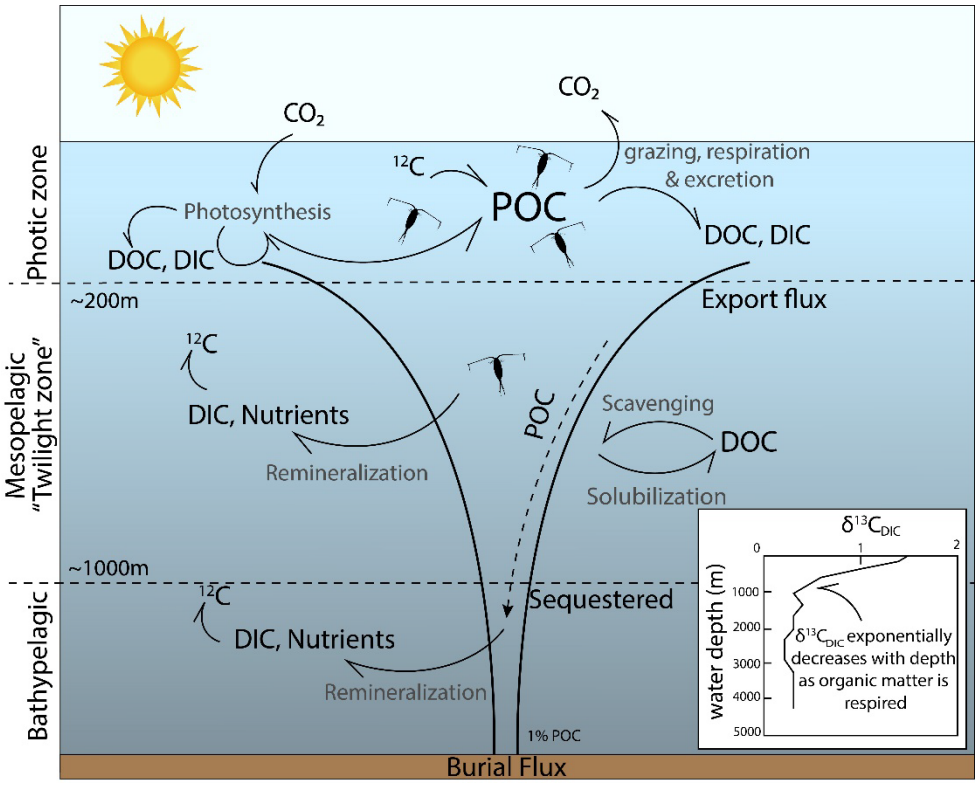

Fig. 1. Illustration of the components of the marine Biological Carbon Pump. Illustration shows the uptake of pCO_2 in surface waters and its transfer to deep waters and deep ocean sediments through the BCP. In the photic zone, primary productivity (photosynthesis) converts dissolved inorganic carbon (DIC) into particulate organic carbon (POC), preferentially utilizing ^{12}C and leaving $\delta^{13}C_{DIC}$-values elevated in the remaining DIC. As POC sinks, microbial respiration remineralizes organic carbon back into DIC, returning isotopically light carbon (^{12}C) to the DIC pool. However, only a fraction (1-40%) of POC is exported from the euphotic zone (<200 m), declining exponentially towards the base of the mesopelagic "twilight zone" (200-1000 m), with a mere fraction (~1%) reaching the ocean interior and deep ocean sediments (Herndl & Reinthaler, 2013). This decline is reflected in the exponential decrease in $\delta^{13}C_{DIC}$-values with depth. The efficiency of the biological carbon pump is controlled by the rate of photosynthesis and export of organic matter out of the photic zone versus its remineralization through the water column. Increased remineralization rates limit the amount of organic matter settling through the water column and reaching the ocean interior and ocean floor, affecting food supply and dissolved oxygen availability at depth.

rates may have contributed to a more efficient and shallow remineralization of POC, consequently decreasing carbon pump efficiency, and food, oxygen and nutrient availability at depth (Boscolo-Galazzo et al., 2018; Crichton et al., 2023; Griffith et al., 2021), potentially even leading to a compaction of the *twilight zone* (Boscolo-Galazzo et al., 2018, 2021; Crichton et al., 2023).

While most research agrees on increased nutrient availability, primary productivity, and carbon sequestration along continental margins (Gibbs et al., 2006; Papadomanolaki et al., 2022; Sluijs et al., 2014; Winguth et al., 2012), the productivity response to PETM warming and carbon cycle perturbations is still controversial for open ocean settings. Geochemical and biotic proxies contradict each other on the direction of change (i.e., increase, decrease, or unchanged) in open ocean productivity during the PETM (Bains et al., 2000; Bralower, 2002; Gibbs et al., 2006; Ma et al., 2014; Moretti et al., 2024; Stoll et al., 2007; Torfstein et al., 2010). This disparity is likely a result of the use of different proxies to reconstruct different components of ocean productivity, and the subsequent

proposed decoupling of these components during the PETM (e.g., Griffith et al., 2021). Additionally, the occurrence of extensive $CaCO_3$ dissolution complicates the reconstruction of accumulation rates and other carbonate dependent components of the marine carbon cycle. Moreover, primary productivity, export production, and the burial of organic matter may have decoupled during the PETM, due to the more efficient remineralization of sinking organic matter related to increased metabolic activity and nutrient utilization rates, changes in local ecosystem structure, and increased oxygen exposure times (e.g., Buesseler, 1998; Griffith et al., 2021; Olivarez Lyle & Lyle, 2006).

The impacts of modern global warming and carbon cycle perturbations on the efficiency of the biological carbon pump are still not well understood. Future projections indicate a decline in marine primary and export production due to increased stratification and reduced nutrient supply, resulting in a decreased organic matter flux to the ocean interior, especially in open ocean settings (Bindoff et al., 2019). Similar processes are expected to have been at play during the PETM, where increased stratification is expected to have led to a decline in biological productivity in open ocean settings (Moretti et al., 2024). Consequently, it is expected that this decline could lead to a reduction in the particulate organic carbon (POC) flux to the benthos by 27-36% in the Atlantic, 31-50% in the Pacific, and 40-55% in the Indian Ocean by 2100 (Sweetman et al., 2017). However, polar regions like the Arctic and Southern Oceans may see increases in net primary and export production, with POC flux potentially rising by 53-60% (Sweetman et al., 2017). By the end of the century, the open ocean is likely to significantly reduce its carbon uptake, especially under the high-emissions RCP8.5 scenario, which is projected to result in a 9-16% decrease in the global carbon settling flux (Bindoff et al., 2019). However, these projections carry only medium confidence due to model uncertainties and the complexity of the biological carbon pump.

Hence, reconstructing these changes for previous periods of rapid and extreme warming and carbon cycle perturbations is important for understanding the carbon cycle and geochemical feedbacks at play in the climate system and the role of the BCP in carbon sequestration during such periods. Therefore, this research attempts to evaluate the change in the efficiency of the soft tissue BCP during the PETM through the reconstruction of vertical carbon isotope gradients (i.e., $\delta^{13}C$-profile) and assess the implications of extreme warming on water column structure, export production and biological activity.

1.3. Physiological Response of Planktic Foraminifera to Warming

The stable carbon and oxygen isotope signature recorded in the shells of planktonic foraminifera is controlled by the isotopic composition of the seawater at the time of calcification, as well as species-specific physiological *vital effects* (e.g., Gaskell & Hull, 2019; Zeebe et al., 1999), such as respiration rate and symbiont photosynthesis. The $\delta^{13}C_{DIC}$-depth profile of paleoseawater can be reconstructed using foraminiferal test derived $\delta^{13}C_{calcite}$, provided the careful consideration of chemical and physiological factors that may result in the departure of $\delta^{13}C$- and $\delta^{18}O$- values from the seawater.

A multitude of factors may cause test isotope values to deviate from DIC including the variability in environmental and ecological factors throughout the foraminifer's lifecycle, such as ontogenic changes in (depth) habitat, thermal structure, food source and supply, and/or seasonal variability and upwelling (Fig. 2; Birch et al., 2013 and references therein). Additionally, size and temperature are known to exert powerful effects on the metabolic rates of planktic foraminifera, which adds another layer of isotopic fractionation (Fig. 2; Birch et al., 2013 and references therein). Size variations, including size changes throughout ontogeny, exhibit an isotopic signature of metabolic depletion in smaller tests sizes (e.g., juveniles) compared to larger tests (e.g., adults), which has been proposed to originate from increased metabolic fractionation rates at smaller shell sizes. (Berger et al., 1978; Birch et al., 2013; Ravelo & Fairbanks, 1995; Spero et al., 1997). Similarly to size, temperature exerts a powerful effect on metabolic rates, which can be encapsulated by the respiratory Q_{10} temperature coefficient, which is the factor by which respiration rate increases per 10 °C increase in ambient temperature. Estimates for the respiratory Q_{10} of photosymbiont-bearing planktonic foraminifera (specifically *G. ruber, G. siphonifera*, and *O. universa*) are approximately 3.18x (Lombard et al., 2009). Furthermore, photosymbiotic fractionation may also contribute to ontogenic isotopic differences, resulting from a logarithmic relationship between test size and symbiont density (Spero &

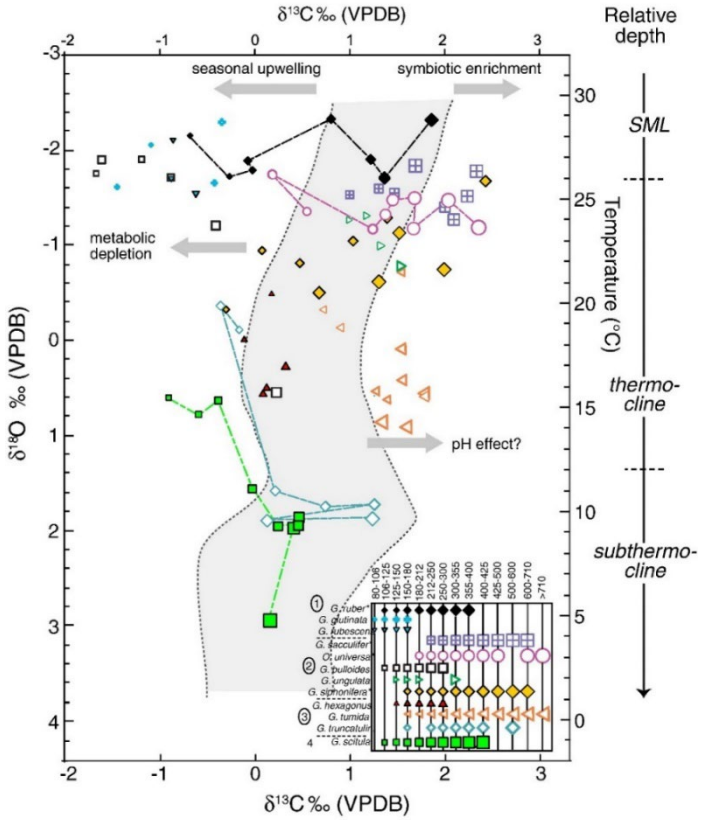

Fig. 2. Expected direction of isotope shift with environmental or physiological change. Illustration shows expected direction of Carbon isotope (δ13C) and oxygen isotope (δ18O) shift with changing environmental (e.g., seasonality, upwelling, living depth) and/or physiological (e.g., metabolic rate, photosymbiont association) factors based on a spread for 12 species of extant planktic foraminifera across a spectrum of test-sizes and habitats. From Birch et al., 2013.

Parker, 1985). Photosymbionts can enrich the shells of photosymbiont-bearing planktic foraminifera in ^{13}C by increased utilization of ^{12}C, and subsequent $H^{13}CO_3^-$ enrichment in the microenvironment surrounding the foraminifer (Spero et al., 1991; Spero & DeNiro, 1987; Spero & Williams, 1988). These photosymbiotic associations also tend to generate a trend of $\delta^{13}C$ enrichment with increasing test size as larger specimens harbor more symbionts. Consequently, symbiont-bearing planktic foraminifera record higher $\delta^{13}C$-values and steeper $\delta^{13}C$-gradients than their asymbiotic counterparts (Spero & Lea, 1993), Lastly, it has been proposed that differential rates in symbiont photosynthesis and metabolism may exert influences on the ambient carbonate ion concentration (pH) local to the planktonic foraminifera (Bijma et al., 1999; Spero et al., 1997; Zeebe et al., 2009b), which may have additional effects on shell isotope signatures.

Rapid changes in marine microfaunal assemblages occurred during the PETM, marked by the most severe extinction of benthic foraminifera in the Cenozoic (e.g., E. Thomas, 2007). This extinction event coincides with a significant turnover in planktic foraminiferal assemblages. One notable change was the shift of tropical foraminiferal assemblages to higher latitudes (Kelly et al., 2002), of which extreme PETM temperatures were likely the principal environmental trigger at driving ecological changes. This turnover also included the emergence of new excursion taxa (e.g., *Acarinina sibaiyaensis* and *Morozovella africana*) and alterations in the relative abundance of planktic foraminifera (e.g., Clay Kelly 1996). Some species of late Paleocene and early Eocene planktic foraminifera are suggested to have relied on algal photosymbionts as they exhibit a similar strong size-$\delta^{13}C$ enrichment as their modern counterparts (D'Hondt et al., 1994; D'Hondt & Zachos, 1993; Kelly et al., 1998). However, under the stress of global warming, photosymbiont activity may have been affected, and potentially even lead to photosymbiont bleaching. This could have negatively affected foraminiferal assemblages and mortality rates, possibly resulting in the temporary exclusion of foraminifera from the geological record in some regions during the PETM (e.g., Aze et al., 2014).

In response, reconstructions of stable carbon and oxygen isotope profiles are expected to reflect these changes in photosymbiont associations. While photosymbiont-bearing planktic foraminifera are important contributors to the open-ocean ecosystem and carbon cycle, the effects of changes in photosymbiont associations in response to climate change are not well understood. It is important to investigate the resilience of these photosymbiont associations to past episodes of extreme warming and carbon emissions to assess the viability of pelagic ecosystems under the influence of modern global warming. Past changes in photosymbiont activity may have distorted the isotope signal recorded in the tests of symbiont-bearing foraminifera, complicating the interpretation of records of past warming events. Consequently, if photosymbiont associations pose particularly vulnerable, and/or symbiont bleaching occurred during the PETM and its effects remain unaccounted for, this could lead to an overestimation of the true carbon isotope excursion due to the superimposed effects of symbiont loss on the apparent CIE.

1.4. Motivation and Research Statement

This thesis aims to conduct a comprehensive analysis on the effects of rapid and extreme warming and carbon cycle perturbations on the efficiency of the marine biological carbon pump and carbon sequestration. The change in the efficiency of the biological carbon pump is assessed through the generation of stable carbon and oxygen isotope data from the tests of photosymbiont-bearing and asymbiotic planktic foraminifera from the South Atlantic (ODP Site 1263, Walvis Ridge), across the rapid warming interval of the Paleocene-Eocene Thermal Maximum. The resilience of photosymbiont-bearing taxa to transient warming episodes is evaluated by analyzing the change in the $\delta^{13}C$- and $\delta^{18}O$-size covariance prior to and during the PETM. Using these size-specific isotope measurements, this study will illuminate on whether these symbiont associations were affected by the geologically abrupt climate perturbations of the PETM. This study on the past warming episode of the PETM aims to provide insight into the potential impacts of sustained global warming on our marine ecosystems and the oceans' capacity to sequester carbon. The overall goal is to develop a better understanding of the long-term consequences of rapid climate change on the role of biological processes and feedback mechanisms in regulating carbon cycling and export within the marine ecosystem.

CHAPTER 2: METHODOLOGY

2.1. Materials

ODP Site 1263 – Location and Lithology

Materials for this study were collected from the southeast Atlantic Ocean Drilling Program (ODP) Site 1263 (28° 31.98'S, 2° 46.77'E) (Fig. 3A). Site 1263 lies on the northeastern flank of the north-south trending ocean ridge segment of *Walvis Ridge* at a water depth of 2,717 m below sea level (mbsl) and paleodepth of roughly 1,500 m (Zachos et al., 2004). Paleogeographic reconstructions place this site at a southern subtropical latitude during the early Eocene (paleolatitude = ~40 °S for Site 1263; Vaes et al., 2023). Site 1263 is particularly well suited for a high-resolution study of planktic foraminifera, as it was cored in four adjacent holes (1263A-D) which yielded a complete and expanded record of Paleogene sediments (Zachos et al., 2004). The recovered sediments consist mainly of nannofossil ooze with good preservation of planktic foraminifera (Zachos et al., 2004), accommodating the high-resolution sampling of planktic foraminifera necessary for the examination of the rapid and transient carbon cycle perturbations associated with the PETM.

The boundary between the Paleocene and Eocene is marked by a transition from carbonate-rich ooze to a dark clay layer, which consequently grades back into carbonate ooze. The dark clay layer is almost completely devoid of carbonate, with a carbonate content of <1 wt % (Fig. 3B). The underlying and overlying carbonate oozes on the contrary measured carbonate contents of 80-95 wt %, consistent with their lower-bathyal open-ocean depositional environment.

Samples studied for this study were collected from sediments recovered from ODP Site 1263A-

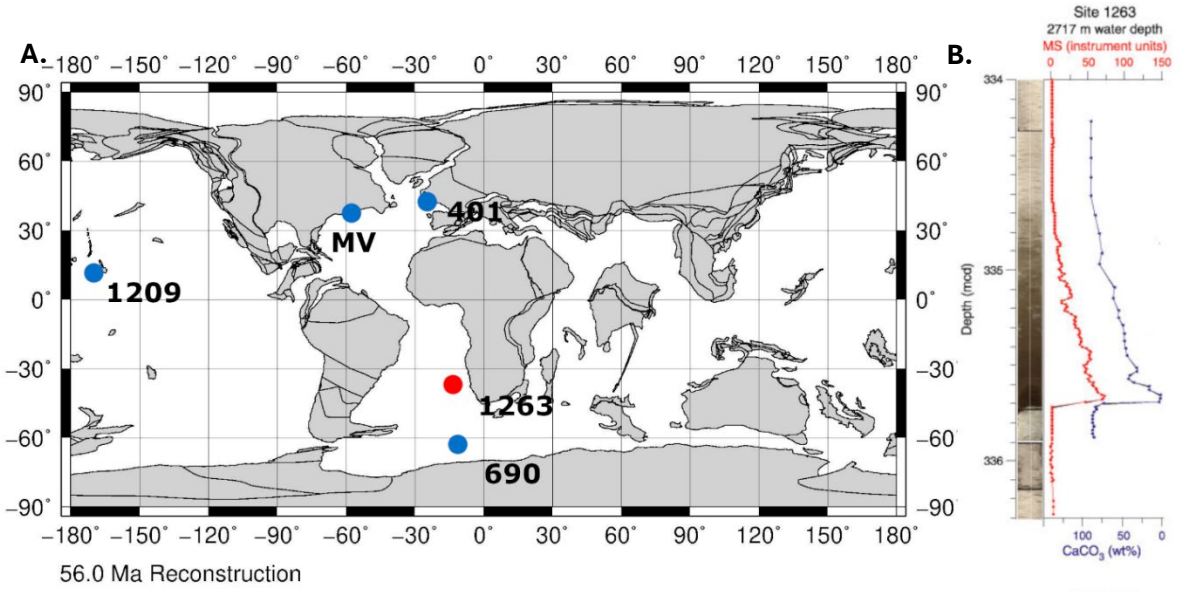

Fig. 3. Figure of locations mentioned in paper. (A) Paleogeographic reconstruction 56Ma showing sites mentioned in this study. **Red** = ODP Site 1263 for which data was generated. **Blue** = ODP Site 1209, ODP Site 690, DSDP Site 401, and Millville (MV). Map from http://www.odsn.de. **(B)** Carbonate content and Magnetic Susceptibility data for from Site 1263 (Zachos et al., 2004).

34X, 1263C-14H, and 1263D-4H. Core depths were calculated by adopting the revised meters composite depth (rmcd) scale composed by Westerhold et al. (2007).

Planktic Foraminifera

To investigate the trends in the planktic foraminiferal response across the PETM, we picked three different genera of planktonic foraminifera, namely *Acarinina*, *Morozovella*, and *Subbotina*. The majority of the picked specimens were of the species *Acarinina soldadoensis*, *Morozovella aequa*, and *Subbotina Patagonia*. However, in cases where material was limited or recrystallization made identification more difficult, we also picked specimens of *A. sibaiyaensis*, *A. coalingensis*, *A. esnaensis*, *M. velascoensis*, *M. subbotinae*, and *M. allisonensis*.

Species of the *Acarinina* and *Morozovella* genera, likely harbored photosymbionts while living at mixed layer depths, as indicated by $\delta^{13}C$-size and $\delta^{18}O$ trends (Aze et al., 2011; D'Hondt et al., 1994; Pearson et al., 2006). In contrast, *Subbotina patagonica* exhibits no size-related increase in $\delta^{13}C$, consistent with an asymbiotic ecology, while oxygen-isotope inferred habitat depths suggests that this taxon occupied the thermocline (Berggren & Norris, 1997; D'Hondt et al., 1994).

Supplementary Data

Supplementary data was collected from prior studies conducted on ODP Site 1263, contributing to a more comprehensive understanding and complete picture of ecological and environmental changes during the PETM. Bulk sediment carbonate content and carbon isotope data were retrieved from Zachos et al. (2005). Furthermore, carbon and oxygen stable isotope data measured on benthic foraminifera (specifically *Nuttallides truempyi* and *Oridorsalis umbonatus*) by McCarren et al. (2008) were utilized to contrast the planktic isotope measurements from this research against benthic values. The newly published record from Moretti et al. (2024) on foraminifera-bound nitrogen stable isotope measurements from Site 1263 were also integrated. Additional data pertaining to the change in the $\delta^{13}C$-size gradient in planktic foraminifera at other sites was also collected from Shaw et al. 2021. This data set encompasses measurements taken from the cores collected at ODP 1209 (Shatsky Rise, Central Pacific), ODP 690 (Maud Rise, Southern Ocean, and DSDP 401 (Meriadzek Terrace, North Atlantic). Additionally, $\delta^{13}C$-size data was collected from previous research on the Millville (New Jersey coastal plain) site (Si & Aubry, 2018).

2.2. Methods

Foraminifera Preparation and Sampling

Planktonic foraminiferal carbon and oxygen stable isotope measurements were generated for ODP site 1263 (South Atlantic). Isotopic analyses were conducted on specimens of species belonging to the planktonic foraminifera genera *Acarinina*, *Morozovella and Subbotina*. To ensure internal consistency and assess size-dependent isotopic trends, analyses focused on foraminifera picked from the restricted size fractions: 150-212 µm, 212-250 µm, 250-300 µm and 300-400 µm. Six depths slices

(namely 334.07, 334.47, 334.67, 335.42, 335.66, and 335.96 rmcd) were chosen for measurements on each of the four size fractions to construct a record of planktic $\delta^{13}C$-size variations through the Paleocene-Eocene transition, while the remaining samples were mainly analyzed at the 250-300 µm size fraction. At this size fraction, shells are fairly abundant throughout the section. Moreover, surface $\delta^{13}C$-values are best estimated using specimens ranging from 212-355µm (Birch et al., 2013).

The planktic foraminiferal specimens were picked from Site 1263 samples taken at roughly 10-20 cm intervals over a 2.6 m interval, from 336.48 rmcd (pre-PETM, 56.09 Mya) to 333.71 rmcd (post-PETM, 55.90 Mya) and subsequently inspected under an optical microscope. To supplement the limited number of planktonic foraminifera available in samples from the core-CIE, planktic foraminifera from adjacent samples were pooled to obtain sufficient material for analyses (minimum of 60 micrograms), albeit resulting in depth-averaging.

Instrumental Setup and Workflow

The multi-specimen carbon and oxygen stable isotope measurements were carried out at the University of South Carolina, utilizing a GasBench II coupled to a continuous flow isotope ratio mass spectrometer (CF-IRMS) (Thermo Scientific Delta-Q). The picked samples were transferred to exetainer vials and loaded onto the GasBench. Each vial contained approximately 60 µg of either sample or reference standard material. The samples were purged with helium for 8 minutes, after which they were injected with approximately 6 drops of phosphoric acid. The samples were then allowed to react with the acid for 50 to 60 minutes in a heated (70°C) rack. Finally, the resulting CO_2 gas was transferred to the respective IRMS for stable isotope measurement through a continuous flow of helium into the exetainer vials.

Carbon and oxygen stable isotope ratios are reported in the delta notation with respect to a reference standard and expressed in permille (‰) (Eq. 1 & 2). Results are reported using the conventional stable isotope delta notation ($\delta^{13}C$ and $\delta^{18}O$) with reference to the Vienna Pee Dee Belemnite (VPDB) standard. The measurements of Carrara marble were used for the standardization of stable isotope measurements. The Carrera marble standard measured average stable isotope values of $\delta^{13}C$ = 1.967‰ (SD = 0.04) and $\delta^{18}O$ = -1.930‰ (SD = 0.07) throughout the runs. The use of standards in stable isotope analyses ensures interlaboratory and long-term instrument reproducibility, stability, and accuracy.

$$\delta^{13}\mathrm{C} = \left(\frac{\left(\frac{^{13}C}{^{12}C}\right)sample}{\left(\frac{^{13}C}{^{12}C}\right)standard} - 1\right) \times 1000 \qquad \textbf{Eq. 1}$$

$$\delta^{18}\mathrm{O} = \left(\frac{\left(\frac{^{18}O}{^{16}O}\right)sample}{\left(\frac{^{18}O}{^{16}O}\right)standard} - 1\right) \times 1000 \qquad \textbf{Eq. 2}$$

Statistical Significance Testing

The p-significance test compares obtained p-values to a preset significance level (α = 0.05),

indicating whether results are statistically significant ($p \leq \alpha$) and justifies the rejection of the null hypothesis (gradient = 0). In our analysis, $\delta^{13}C$-size gradient p-values were calculated in R to assess the statistical significance of $\delta^{13}C$-size gradients across the PETM.

Age Model

The age model produced by Röhl et al. (2007) was used in this study to generate the age-depth correlation used in this study. The age model was used to produce relative ages to the onset of the CIE, which were subsequently converted to absolute ages, assigning an age of 56.01 Ma (Zeebe & Lourens, 2019) to the base of the CIE. Linear interpolation was used between tie points to calculate the age of each depth sample.

CHAPTER 3: RESULTS

3.1. Sample and Assemblage Descriptions.

Foraminiferal Assemblage

Various species of the genera *Acarinina*, *Morozovella*, and *Subbotina* were picked, the most abundant species of which were *Acarinina soldendoeansis*, *Morozovella aequa*, *Morozovella velascoensis*, and *Subbotina Patagonica*. The relative abundance of the three genera varied throughout the core, however it should be noted that Site 1263 was not subjected to a true study of relative abundance. Nevertheless, a general preliminary trend was discerned across the PETM. Below the dissolution horizon, marking the onset of the CIE, the relative abundance of each taxa seemed relatively similar across all samples, with *Acarinina ssp.* and *Subbotina* appearing slightly more abundant compared to *Morozovella ssp.* However, the relative abundance of these genera in the post-dissolution CIE samples showed to be distinctly different. Samples recovered from the CIE interval revealed that *Acarinina ssp.* was by far the most abundant, while the relative abundance of *Subbotina* was noticeably decreased. This decreased relative abundance of *Subbotina* compared to the photosymbiont-bearing genera during the CIE is consistent with previous studies at different localities during the PETM (e.g., Hupp et al., 2022; Pardo et al., 1997; Shaw et al., 2021)

The foraminifera picked for analysis were generally in good condition, with frosty wall texture and little visible secondary calcite recrystallization. Generally, the CIE samples were more recrystallized compared to pre- and post-CIE shells. Most samples were depleted in benthic foraminifera, as the samples had been previously selected for research at ODP Site 1263.

Physical Description of Core Samples

The physical appearance of the samples varied with depth. Pre-CIE samples were notably rich in planktic foraminifera, clay, and calcium carbonate structures. The base of the CIE was easily recognized due to its near absence of fossil and calcium carbonate material. The scarcity in sample material is likely attributable to the increased dissolution of carbonate structures and the shoaling of the carbonate compensation depth (CCD) during the PETM (Zachos et al., 2005). These processes led to the compaction of seafloor sediments during the PETM, resulting in the reduced availability of sediments and organic matter throughout the CIE. Upwards through the CIE, the samples notably increased in fossil and carbonate content, likely coinciding with the PETM recovery phase. Interestingly, the samples at the base of the CIE were comparably more abundant in fish teeth. Generally, the samples at the base of the CIE were poorly preserved, with very fragmented and sometimes very remineralized foraminiferal tests. The secondary growth of calcite, especially on specimens of Acarinina, seemed to be mainly an issue for the samples at the base of the CIE, while pre- and post-CIE samples, as well as those collected from the recovery interval, appeared to be in pristine condition.

3.2. Stable Isotope Measurements

Size-specific carbon and oxygen stable isotope measurements were generated on planktic foraminifera from Site 1263 (Fig. 4). The characteristic negative carbon isotope excursion recorded is useful to distinguish the PETM into four stratigraphic intervals: pre-CIE, core/peak-CIE, CIE-recovery, and post-CIE interval. The onset of the CIE is missing from our measurements. The first excursion value is recorded at a depth of 334.65 rmcd. However, this depth does not correspond to the onset of the CIE. The samples between the onset of the carbonate dissolution (335.27 rmcd) and the first recorded excursion value (334.65 rmcd), were very depleted in planktic foraminifera. This depletion was likely caused by the high rate of carbonate dissolution at the base of the CIE, and impeded the measurement of foraminiferal tests for the base of the CIE. Consequently, it is anticipated that our data underestimates the magnitude of the CIE due to the absence of its onset.

Carbon and Oxygen Stable Isotope Excursion

The carbon isotope excursion recorded between pre-CIE samples and core-CIE samples shows interspecies variability (Table 1). The largest carbon isotope excursion is recorded by the surface-dwelling, photosymbiont-bearing foraminifera *Acarinina* ($\Delta\delta^{13}C$ = –2.65‰) and *Morozovella* ($\Delta\delta^{13}C$ =

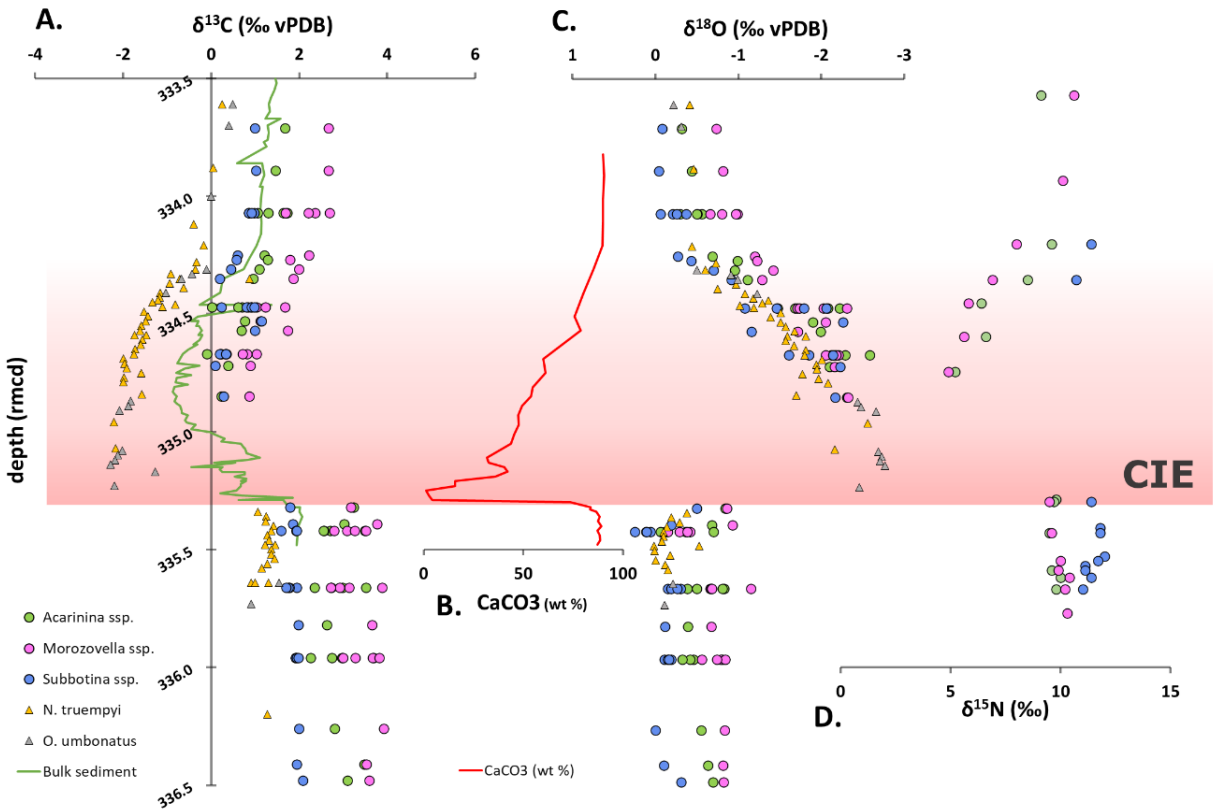

Fig. 4. Compilation of data sets (A) Newly generated planktic $\delta^{13}C$ isotope record (circles) paired with benthic foraminifera (triangles, McCarren et al., 2008) and bulk sediment (green line; Zachos et al., 2005) $\delta^{18}O$ measurements. **(B)** Calcium Carbonate ($CaCO_3$) content (wt %) (Zachos et al., 2005). **(C)** Newly generated $\delta^{18}O$ planktic foraminifera data (circles) and benthic foraminifera data (triangles; McCarren et al., 2008). **(D)** Planktic foraminifera; nitrogen isotope ($\delta^{15}N$) measurements from Moretti et al., 2024.

–2.53‰). Specimens of the thermocline-dwelling asymbiotic *Subbotina* record the lowest excursion value across the PETM ($\Delta\delta^{13}C$ = –1.68‰).

Table 1. Average values of the carbon and oxygen stable isotope measurements of the 250-300 µm size fraction. Values are calculated individually for *Acarinina*, *Morozovella* and *Subbotina*. Excursion values represent the isotopic difference between the pre-CIE (336.48 to 335.32 rmcd) and the core-CIE (334.85 to 334.67 rmcd). The CIE-recovery is excluded from averaging, due to its high variance in isotope values during the gradual recovery from the core-CIE to post-CIE values.

	pre-CIE		CIE		post-CIE		Excursion	
species	$\delta^{13}C$	$\delta^{18}O$	$\delta^{13}C$	$\delta^{18}O$	$\delta^{13}C$	$\delta^{18}O$	$\Delta\delta^{13}C$	$\Delta\delta^{18}O$
Acarinina	2.824	-0.506	0.170	-2.189	1.018	-1.117	-2.653	-1.683
Morozovella	3.348	-0.702	0.823	-2.218	1.919	-1.385	-2.525	-1.516
Subbotina	1.917	-0.170	0.239	-1.999	0.675	-0.711	-1.678	-1.829

A similar excursion is distinguished in the oxygen stable isotope record, although with less variability between species (Table 1). Maxima in $\delta^{18}O$ are recorded just before the onset of the CIE at a depth of 335.42 rmcd. The largest excursion is recorded in *Subbotina* with a depletion of $\Delta\delta^{18}O$ = –1.83‰ compared to pre-CIE values. *Acarinina* and *Morozovella* record a slightly less depleted excursion of $\Delta\delta^{18}O$ = –1.68‰ and $\Delta\delta^{18}O$ = –1.51‰, respectively.

Duration and Recovery of the CIE

The CIE onset occurs at 335.27 rmcd (56.01 Mya). The CIE core, from the onset to initial recovery is estimated to have lasted ~58 kyr, based on the age model used (Fig. 5). The initiation of the recovery interval is placed at 334.67 rmcd (~55.952 Mya), after which $\delta^{13}C$-values start to gradually increase up to 334.25 rmcd (~55.921 Mya). The oxygen isotopes also show a gradual recovery to values similar to pre-CIE values. This recovery is estimated to have lasted around ~41 kyr, based on the age model used (Fig. 5). The same gradual recovery trend is recognized in the isotope records of bulk sediment, benthic foraminifera and planktic foraminifera-bound nitrogen, as well as in carbonate content measurements.

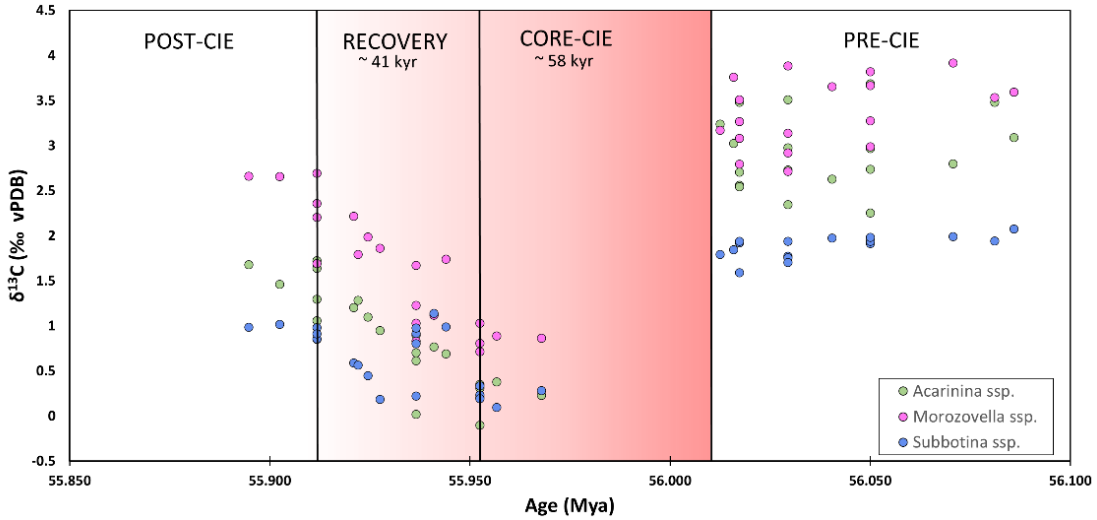

Fig. 5. Constructed age model with carbon stable isotope measurements for ODP Site 1263. Onset of the CIE is missing due to low fossil abundance. Estimated duration of core-CIE is ~58 kyr and ~41 kyr for the recovery interval.

A note should be made on the discrepancy in duration between this study and the 150-250 kyr duration of the CIE as measured by Murphy et al. (2010), Röhl et al. (2007) and Zeebe & Lourens (2019). This discrepancy arises from a different "break up" of the CIE into three phases, i.e., the "core", and two recovery phases (i.e., phase 1 and phase 2). This study defined the "core"-interval as starting at the onset of the CIE up to where $\delta^{13}C$ starts to increase again, which is one cycle earlier than other definitions (e.g., Murphy et al., 2010; Röhl et al., 2007). This difference in the definition of the core-CIE builds into the second dissimilarity, which is the definition of the recovery interval. This study's "recovery"-interval matches with phase 1 and the last cycle of their "core"-interval. Based on these differences, our "core"-interval should constitute of three precession cycles, while our "recovery"-interval should constitute of two precession cycles to match previous estimations. These durations match our age-model estimates for a 58-kyr core-CIE and 41-kyr recovery period.

Interspecies Isotopic Gradient

The discrepancy in the magnitude of the excursion recorded by the mixed layer and thermocline dwelling species causes the apparent interspecies convergence of $\delta^{13}C$-values during the CIE (Table 1; Fig. 4 and 6). In the pre-CIE samples, *Morozovella* consistently plots the highest $\delta^{13}C$ values, while *Subbotina* records the lowest $\delta^{13}C$-values. However, this trend is diminished during the CIE, during which the $\delta^{13}C$-gradient between all three taxa is significantly reduced. The most pronounced reduction in interspecies $\delta^{13}C$-gradient is observed between *Acarinina* and *Subbotina*, owing to the fact that during the CIE, *Acarinina* plots $\delta^{13}C$-values remarkably similar to those of *Subbotina*. The collapse in the interspecies $\delta^{13}C$-gradient between surface-dwelling, photosymbiont-bearing foraminifera, and thermocline-dwelling, asymbiotic *Subbotina* has also been observed at other localities (e.g., Shaw et al., 2021). The $\delta^{13}C$-gradient between planktic and benthic foraminifera at Site 1263 seems to increase during the CIE, with benthic foraminifera recording a larger excursion (Fig. 4 and 6), a pattern that is not observed in other sites.

Although less pronounced, the $\delta^{18}O$-gradient between planktic foraminifera is also reduced during the CIE. Before the excursion, $\delta^{18}O$ values of *Morozovella*, *Acarinina* and *Subbotina* show clearly contrasting values. During the CIE however, the $\delta^{18}O$-gradient is reduced, with all three genera recording oxygen stable isotope values around -2.1‰ (Table 1; Fig. 4 and 6). Prior to and following the CIE, *Subbotina* consistently records the highest $\delta^{18}O$-values, while *Morozovella* consistently records the lowest $\delta^{18}O$-values, reflecting their relative positions in the water column. However, during the CIE, this trend is diminished as the lowest (warmest) $\delta^{18}O$-values are recorded by all three genera depending on the sample analyzed.

Cross plots of $\delta^{13}C$ versus $\delta^{18}O$ show a distinct trend between the stable carbon and oxygen isotopes before and after the CIE (Fig. 6a). This trend can be described as a negative trend, with higher $\delta^{13}C$-values corresponding to lower $\delta^{18}O$-values. During the CIE, this linear relationship all but disappears.

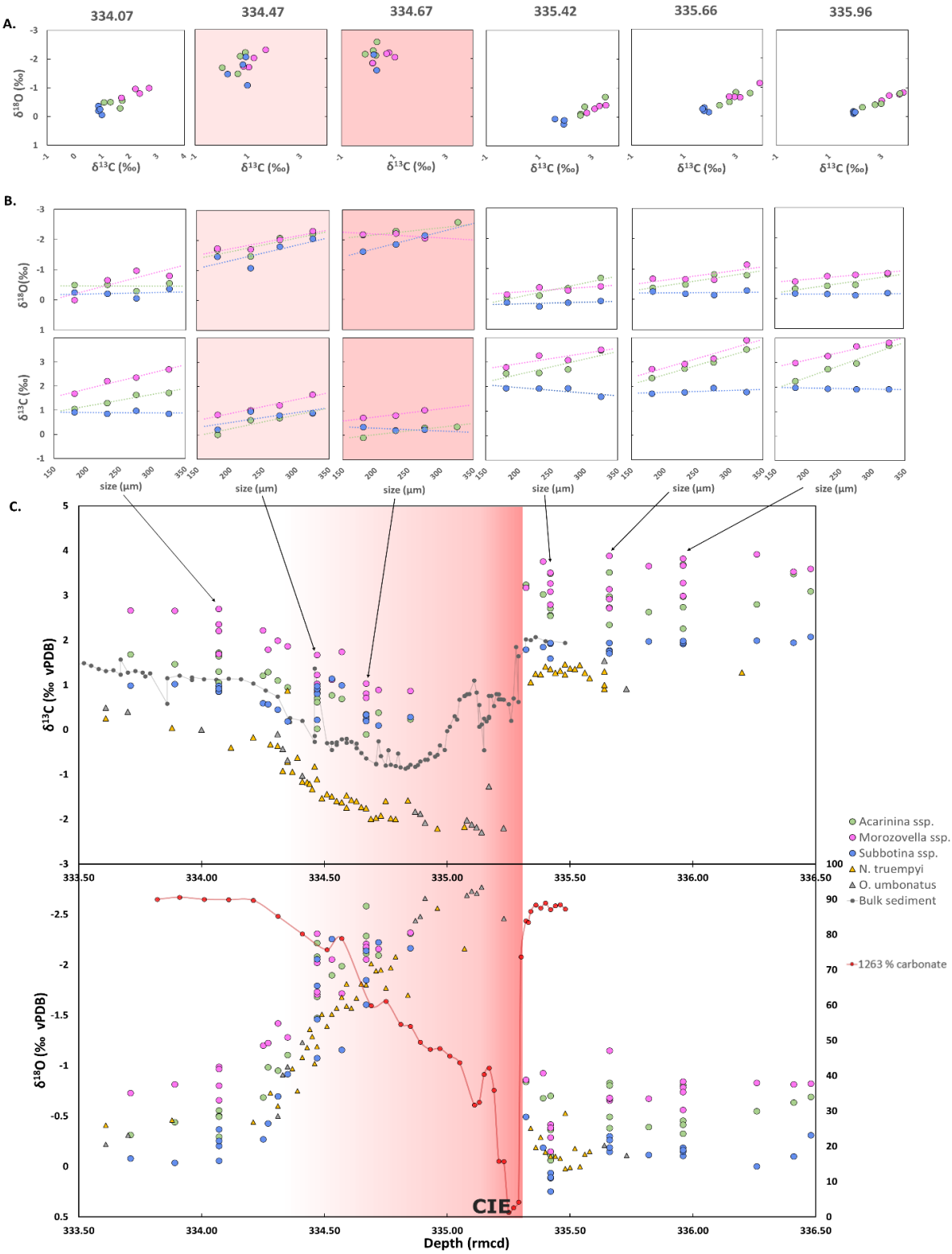

Fig. 6. Size dependence in isotope measurements (A) $\delta^{13}C$ versus $\delta^{18}O$ for the six depth slices. **(B)** $\delta^{18}O$ (top) and $\delta^{13}C$ (bottom) versus test size **(C)** Compilation of $\delta^{13}C$ (top) and $\delta^{18}O$ (bottom) measurements of planktic and benthic foraminifera, bulk sediment, and carbonate content for Site 1263 (right axis).

Size-$\delta^{13}C$ Gradient Response

A positive relationship between $\delta^{13}C$ and test-size is discerned in *Acarinina* and *Morozovella* across all depths (Fig. 6b). This trend is consistent with the external hosting of photosymbionts, similarly to extant planktic foraminifera (D'Hondt et al., 1994; Gaskell & Hull, 2019). The slope in the $\delta^{13}C$-gradient (i.e., $\Delta\delta^{13}C$ between the largest and smallest test-size) of these species is significantly reduced during the core of the CIE compared to pre-CIE gradients (Table 2; Fig. 6b). On average, the size-$\delta^{13}C$ slopes of the photosymbiotic species are the steepest during the pre-CIE interval and shallowest during the core of the CIE. In contrast, the $\delta^{13}C$-values derived from *Subbotina* tests do not appear to correlate to any significant size-$\delta^{13}C$ trend, which agrees with an asymbiotic lifestyle (D'Hondt et al., 1994).

Changes in the $\delta^{18}O$-size gradient are also observed through the PETM (Table 2; Fig 5b). *Subbotina* shows no gradient before and after the CIE. However, during the CIE, *Subbotina* shows more negative (warmer) $\delta^{18}O$ values with size. *Morozovella* shows an opposite trend in the core-CIE sample, registering colder $\delta^{18}O$-values with size. In contrast, during the recovery phase and after the CIE *Morozovella* shows a strong gradient registering warmer values throughout ontogeny. *Acarinina* shows a reduced gradient during the CIE and the development of a stronger gradient during the recovery phase.

3.3. Statistical Significance Tests

The significance (*p*-value) of the size dependent slopes varies between samples (Table 2). The $\delta^{13}C$-size slopes of *Acarinina* and *Morozovella* are the most statistically significant before the onset of the CIE. Their significance is reduced in the sample taken from just before the CIE (335.42 rmcd) and during the core-CIE (334.67). The CIE-recovery and post-CIE samples record more significant slopes for *Morozovella* than for *Acarinina*. The overall pattern shows reduced $\delta^{13}C$-size slopes during the core-CIE, although their uncertainty should be considered. Regression slopes were insignificant in *Subbotina* across all depths due to the absence of size-$\delta^{13}C$ enrichment. The $\delta^{18}O$-size gradients are mostly insignificant, likely due to the susceptibility of $\delta^{18}O$-values to remineralization and their typically lower slopes. Considering this, overarching trends will still be explored and discussed.

Table 2. $\delta^{13}C$ (top) and $\delta^{18}O$ (bottom) test size gradient. Difference between largest and smallest test sizes denoted in Δδ. Slopes are measured in permille per 100 µm. *P*-values indicate the significance of slopes. Note: 334.67 largest test-size is 250-300 µm instead of 300> µm. The smallest test-size is constant between all depths. Depths are given in rmcd for site 1263.

		Acarinina			*Morozovella*			*Subbotina*	
Depth slice (rmcd)	**$\Delta\delta^{13}C$**	***slope (‰/100 µm)***	***p***	**$\Delta\delta^{13}C$**	***slope (‰/100 µm)***	***p***	**$\Delta\delta^{13}C$**	***slope (‰/100µm)***	***p***
334.07 (post-CIE)	0.667	0.408360	0.05501	1.002	0.56410	0.03008	-0.063	-0.01944	0.77180
334.47 (CIE-recovery)	0.877	0.477400	0.09504	0.838	0.49811	0.00514	0.692	0.32900	0.31620
334.67 (core-CIE	0.452	0.252040	0.11970	0.317	0.33386	0.17040	-0.103	-0.11350	0.47760
335.42 (pre-CIE)	0.937	0.594600	0.17770	0.717	0.38450	0.26350	-0.348	-0.21934	0.16170
335.66 (pre-CIE	1.166	0.680810	0.00116	1.172	0.69560	0.02469	0.067	0.05394	0.61720
335.96 (pre-CIE)	1.434	0.829120	0.00454	0.830	0.50540	0.03719	-0.067	-0.03800	0.10030

		Acarinina			*Morozovella*			*Subbotina*	
Depth slice (rmcd)	**$\Delta\delta^{18}O$**	***slope (‰/100 µm)***	***p***	**$\Delta\delta^{18}O$**	***slope (‰/100 µm)***	***p***	**$\Delta\delta^{18}O$**	***slope (‰/100µm)***	***p***
334.07 (post-CIE)	-0.06	-0.013590	0.91540	-0.331	-0.15320	0.29070	-0.116	-0.05718	0.68400
334.47 (CIE-recovery)	-0.533	-0.393100	0.18250	-0.577	-0.37415	0.05291	-0.594	-0.45460	0.23170
334.67 (core-CIE	-0.423	-0.221400	0.24850	0.126	0.12970	0.47280	-0.535	-0.56722	0.05845
335.42 (pre-CIE)	-0.639	-0.399020	0.13930	-0.268	-0.13470	0.41100	-0.043	-0.04875	0.70840
335.66 (pre-CIE	-0.424	-0.275000	0.12200	-0.467	-0.27410	0.18010	-0.038	-0.02363	0.75740
335.96 (pre-CIE)	-0.482	-0.280650	0.04793	-0.281	-0.15588	0.07849	-0.024	-0.01106	0.76710

CHAPTER 4: DISCUSSION

4.1. Evaluation of the CIE as Recorded in Planktic Foraminifera

The changes discerned in inter- and intraspecies carbon and oxygen isotope gradients can provide valuable insights into the processes that maintain these gradients. At Site 1263, the magnitude of the CIE is restricted to roughly –2.6‰ in *Morozovella* and *Acarinina,* and –1.7‰ in *Subbotina* (Table 1, Fig 3 and 5c). The excursion measured in oxygen stable isotopes shows a drop of on average –1.7‰ across all three genera (Table 1, Fig. 4 and 6c). These excursion values are consistent with published records for the carbon and oxygen isotope excursion in planktic foraminifera across the PETM (e.g., Hupp et al., 2022; Shaw et al., 2021; Thomas et al., 2002; Zachos et al., 2003). Based on an approximate decrease of 0.25‰ $\delta^{18}O$ per 1 °C increase in temperature, we roughly estimate a temperature increase of 6-7 °C (1.5-1.8‰) during the PETM. These values may underestimate SST warming due to a possible downwards migration by mixed-layer taxa as a response to PETM warming (e.g., Si & Aubry, 2018). Benthic foraminiferal data from Site 1263 (Fig. 4 and 6c), suggests a possible 10 °C warming at the onset of the CIE (McCarren et al., 2008). The extreme carbonate dissolution during the initial stages of the PETM (e.g., Zachos et al., 2005) dissolved all planktic foraminifera. Nevertheless, it is likely that more negative excursion values would be observed at the base of the CIE, suggesting that the magnitude proposed in this (and other) study serves as a conservative minimum baseline for the excursion at Site 1263.

The high $\delta^{13}C$ and low $\delta^{18}O$ signatures recorded in pre-CIE *Morozovella* and *Acarinina* tests indicate and confirm that these taxa inhabited the mixed layer surface waters, while the relatively low $\delta^{13}C$ and high $\delta^{18}O$ signature recorded in *Subbotina*, confirms their occupancy of deeper, more-depleted thermocline waters. During the PETM, the isotopic signatures recorded in these foraminifera changed relative to pre-CIE conditions. The change in the linear relationship between $\delta^{13}C$ and $\delta^{18}O$ as recorded in planktic foraminifera (Fig. 6a), suggests a disturbance in carbon and oxygen isotope space during the CIE as a result of surface ocean warming, the uptake of ^{13}C-depleted carbon, or changes in foraminifera ecology and/or metabolic physiology.

4.2. PETM Changes in $\delta^{13}C$- and $\delta^{18}O$-Gradients

The carbon and oxygen isotopic gradients between surface- (*Morozovella* and *Acarinina*) and thermocline-dwellers (*Subbotina*) reflects the strength of the thermocline ($\Delta\delta^{18}O$) and biological carbon pump ($\Delta\delta^{13}C$) (Dunkley Jones et al., 2013; John et al., 2013). Prior to the CIE, this gradient is around 1-1.5‰ in $\delta^{13}C$, and 0.5‰ in $\delta^{18}O$ (Table 1). During the CIE, both $\delta^{13}C$ and $\delta^{18}O$ gradients are reduced to <0.6‰ in $\delta^{13}C$ and 0.2‰ in $\delta^{18}O$ (Table 1). This reduction in the surface-to-thermocline $\delta^{13}C$- and $\delta^{18}O$-isotopic gradients could indicate (1) a migration of planktic foraminifera to similar depths, or (2) a disruption in the physical and isotopic structure of the surface ocean and thermocline. The collapse in the interspecies gradient between *Morozovella* and *Subbotina* is slightly less pronounced compared to *Acarinina* and *Subbotina*. These results indicate a slightly greater separation and sustained

offset between *Morozovella* and *Subbotina*, and are possibly suggestive of a moderately greater resilience of *Morozovella* to PETM environmental perturbations with respect to *Acarinina*.

The collapse in the surface-to-thermocline $\delta^{13}C$-isotopic gradients may have been intensified by a change in photosymbiont activity. The intraspecies $\delta^{13}C$-size gradient recorded in *Acarinina* and *Morozovella* reflects the strength of photosymbiotic associations. Both taxa display a reduction in the size-dependent $\delta^{13}C$-gradient (Fig. 6b), although this decrease appears more pronounced in *Acarinina*. Therefore, it is possible that during the PETM a decrease in photosymbiont activity and/or its importance to the foraminifer's metabolism occurred. Another possibility is that temperature induced stress caused photosymbiont bleaching in these taxa. However, such a scenario is difficult to reconcile with records of increased relative abundance of photosymbiont-bearing taxa relative to asymbiotic taxa during the PETM (e.g., Hupp et al., 2022; Pardo et al., 1997; Shaw et al., 2021).

The $\delta^{18}O$-size gradient reflects the vertical migration of a species during ontogeny. Pre-PETM data shows no vertical migration in *Subbotina* through ontogeny (Fig. 6b). During the PETM, the establishment of a stronger $\delta^{18}O$-size gradient indicates that *Subbotina* may have inhabited shallower depths through ontogeny during the CIE. For *Morozovella*, the $\delta^{18}O$ depletion with increasing test size suggests migration towards relatively shallower habitats throughout ontogeny before and after the PETM. This trend is reversed within the CIE. *Acarinina* also shows a reduced gradient during the CIE, which may indicate a narrower depth habitat. The strong $\delta^{18}O$-size gradient discerned during the recovery phase in *Acarinina* and Morozovella may indicate their repopulation of a wider depth range.

The observed increase in the $\delta^{13}C$-gradient between planktic and benthic foraminifera during the PETM suggests enhanced depletion of deep ocean $\delta^{13}C_{DIC}$ and/or enrichment of surface ocean $\delta^{13}C_{DIC}$. This could occur with a reversal of deep ocean circulation as is suggested by increases in seafloor carbonate dissolution in the S. Atlantic relative to the Pacific (Zeebe & Zachos, 2007), causing the waters at Walvis Ridge to be sources from older and more depleted waters Nunes & Norris, 2006). Alternatively, increased surface ocean $\delta^{13}C$ may stem from heightened primary productivity, implying higher nutrient availability, potentially due to enhanced silicate weathering (Brault et al., 2017; Kelly et al., 2005; Penman, 2016; Zachos et al., 2005), or more efficient turnover. However, most other evidence supports a decline in export production.

4.3. Current Hypotheses for Changes in Surface-to-Thermocline Isotopic Gradients

Three general hypotheses have been proposed to explain the reduction in the $\delta^{13}C$-gradient between the surface mixed layer and thermocline waters during the peak CIE (Fig. 7); (1) a change in ocean circulation/mixing, (2) temperature-induced depth migration of surface dwellers and associated loss of photosymbionts, or (3) a change in the efficiency of the biological carbon pump at remineralizing organic matter.

Hypothesis 1 attributes the changes in $\delta^{13}C$-profile to a major shift in ocean circulation and

mixing. A transient breakdown in ocean stratification may have caused an enhanced mixing of $\delta^{13}C$ between surface and deeper water, as well as a collapse in the thermocline ($\delta^{18}O$-gradient) (Thomas et al., 2002; Thomas & Shackleton, 1996). Such a breakdown in ocean stratification may have been a result of a change of deep-water formation. It is theorized that the warming of the PETM may have triggered changes in ocean circulation, such as the switch of SH overturning to NH overturning, rendering a warming of the intermediate waters in the southern Atlantic (Bice & Marotzke, 2002; Lunt et al., 2010; Nunes & Norris, 2006). However, ODP 1263 and other open ocean sites (e.g., ODP 1209), have been suggested to exhibit signs of increased oligotrophy and enhanced stratification (e.g., Schneider et al., 2013), while also recording a collapse in the carbon and oxygen isotopic gradients (Petrizzo, 2007).

For hypothesis 2, the collapse in the surface-to-thermocline $\delta^{13}C$-gradient observed at Site 1263, and other sites (e.g., Shaw et al., 2021; Si & Aubry, 2018), is attributed to depth migration by surface dwellers to deeper waters (Si & Aubry, 2018), where $\delta^{13}C$ of seawater is more depleted compared to the mixed layer surface waters. Extreme PETM warming, high pCO_2, and lower surface ocean pH could all have acted as stressors, compelling surface dwellers to migrate to deeper, colder depths (Si & Aubry, 2018). The initiation of depth migrations in planktic foraminifera is not unprecedented in previous geological warming episodes (e.g., Coxall et al., 2007; Matsui et al., 2016). Migration of photosymbiont-bearing taxa out of the euphotic zone are anticipated to have triggered a substantial decrease in photosymbiont activity.

However, the artificial suppression of photosymbiont activity on species of photosymbiont-bearing planktic foraminifera, revealed their struggle to survive at depths below the euphotic zone for extended periods of time (Bé et al., 1982), illuminating the significance of light availability on their survival. Hence, the theoretical migration of these taxa to deeper waters during the PETM would

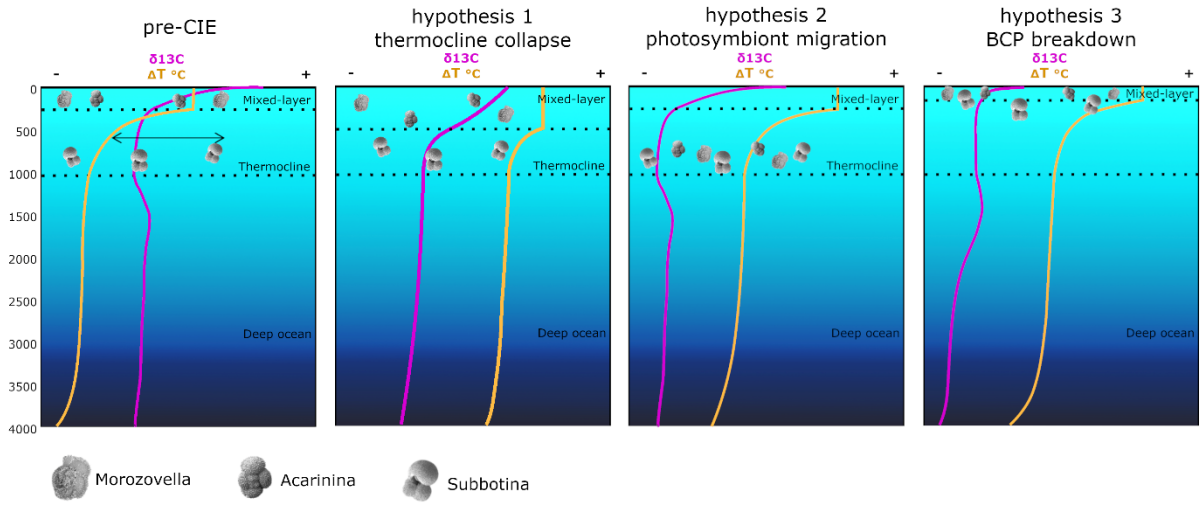

Fig. 7. Illustration of carbon and oxygen isotope gradients throughout the water column (pre-CIE and hypothesis). Depicted are the responses of the carbon and oxygen isotope gradients and planktic foraminiferal depth habitats to the pre-CIE and hypothesized conditions. Hypothesis 1: breakdown in thermocline strength and stratification; hypothesis 2: depth migration in photosymbiont bearing foraminifera from mixed layer to thermocline; hypothesis 3: transient breakdown in biological carbon pump efficiency.

logically coincide with a rise in mortality rates. However, the persistence of $\delta^{13}C$-size gradients in photosymbiont-bearing taxa and the observation that these taxa are suggested to have thrived relative to asymbiotic taxa, indicates that photosymbiont associations remained of great important to the survival of these taxa during the PETM.

Hypothesis 3 attributes the collapse in the isotopic gradients to a less efficient marine biological carbon pump, resulting from an increase in the temperature-dependent remineralization of organic matter. If the Q_{10} values of symbiont-bearing planktic foraminifera were around 3 (estimate based on Lombard et al., 2009), respiration rates could have doubled during the CIE (+ 6-7 °C). Increased remineralization rates are suggested to have driven the rapid depletion in $\delta^{13}C_{DIC}$ with depth, and consequently caused a shallower and sharper depletion in $\delta^{13}C_{calcite}$. If biogenic remineralization operated with greater efficiency during the PETM, the transport of organic matter and nutrients to the twilight zone and benthos would likely have been greatly reduced. This nutrient and export depletion was likely exacerbated by the increased stratification of the surface ocean during the PETM. This decline in organic matter reaching deep ocean sediments, along with the shoaling of the CCD, likely reduced the carbon sequestration capacity in the open ocean. This theory is supported by the observed decreased abundance and biodiversity in benthic foraminifera during the PETM (Thomas & Shackleton, 1996), indicating the harsher bottom water conditions at Site 1263.

Moreover, the implications of a shallower depth of remineralization suggests a narrower mixed-layer depth habitat for *Morozovella* and *Acarinina* (Fig. 7), consistent with the relative reductions observed size gradients. Furthermore, the combined effects of warming and increased oligotrophy within the *twilight zone* may have led to less feasible conditions for *Subbotina*, hence leading to their decreased relative abundance. It is conceivable under this scenario that *Subbotina* migrated towards shallower depths as an adaptive response to reduced export production and sparse food and nutrient availability at depth. This idea is supported by the development of a stronger $\delta^{18}O$-size gradient in *Subbotina*, suggesting the migration to shallower depths throughout their life cycle.

Recently published foraminifera bound $\delta^{15}N$ data for the PETM has been used to infer changes in upper ocean redox conditions as influenced by export production. Data from Site 1263 shows a significant decrease in planktonic foraminifer $\delta^{15}N$ (Moretti et al., 2024; Fig. 4). Similar $\delta^{15}N$ enrichments are recorded at Site 1209, Site 213 (Indian Ocean), and Site 690. Moretti et al. (2024) attributes the increase to a decrease in denitrification rates as a result of an increase in subsurface oxygen availability. If hypothesis 3 holds true and the efficiency of the marine biological pump decreased during the PETM – which is deemed likely by the collapse in the surface-to-thermocline $\delta^{13}C$-gradient collapse – the increased remineralization rate in the mixed layer would infer a decrease in export production to the ocean interior. The resulting decreased oxygen utilization rates in the ocean interior would thereby increase oxygen availability at depth. Moreover, the reduced flux of organic particles to depth might also force deeper dwellers such as Subbotina to migrate upward thus further

reducing the C isotope gradients.

4.4. Spatial Comparison and Variation in Planktic Isotopic Gradient Changes

Previous studies on the response of planktic foraminifera and photosymbiont associations suggest a spatially varied response to PETM environmental perturbations (Fig. 8). At ODP Site 1209 (Shatsky Rise, Central Pacific), there is a notable species-specific response to the PETM. During the PETM, the $\delta^{13}C$-gradient between *Acarinina* and *Subbotina* collapses completely, while *Acarinina* also loses its $\delta^{13}C$-size gradient. Markedly, *Morozovella* retains its $\delta^{13}C$-size gradient and continues to plot higher $\delta^{13}C$-values, showing no signs of a change in photosymbiont associations. At DSDP 401 (Meriadzek Terrace, North Atlantic), specimens do not show any sign of a significant interspecies $\delta^{13}C$-gradient collapse. The positive size-$\delta^{13}C$ relationship occurs in *Acarinina* and *Morozovella* throughout the PETMS, although *Acarinina* shows slightly reduced $\delta^{13}C$-size gradients, with no discernable changes in photosymbiont associations for *Morozovella*. At ODP 690 (Maud Rise, Southern Ocean), interspecies gradients between *Acarinina* and *Subbotina* are dramatically reduced at the onset of the PETM, after which they gradually recover through the remainder of the CIE. Furthermore, ODP Site 690 (Maud Rise, Southern Ocean) and the New Jersey coastal plain site (Millville) both exhibit an increased $\delta^{13}C$-size

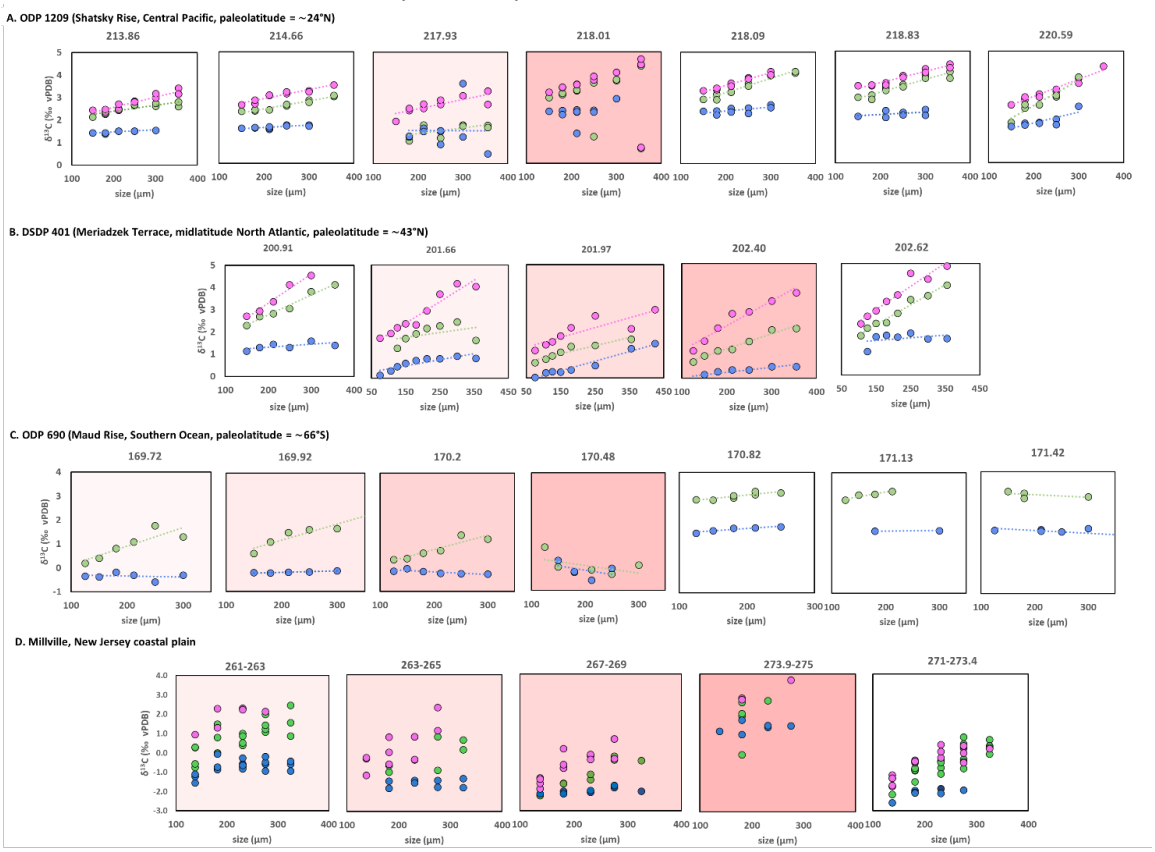

Fig. 8. $\delta^{13}C$-size data from additional sites. ODP 1209 (Shatsky Rise), 690 (Maud Rise), 401 (Meriadzek Terrace), and Millville (New Jersey coastal plain) planktonic foraminifera test size-$\delta^{13}C$ data for subspecies of Acarinina (green), Morozovella (pink), and Subbotina (blue). Red (darkness) = CIE interval intensity, interval depths become shallower and younger towards the left. Depths depicted in mbsf. Sample 218.01 at ODP 1209 was likely subjected to mixing and/or coring disturbance. Data collected from Shaw et al. (2021) and Si and Aubry (2018)

gradient and collapse in the interspecies $\delta^{18}O$-gradient during the CIE interval compared to pre-CIE conditions. It has been proposed that some of the observed changes in isotope gradients at ODP 690 are artifacts of deposition (Hupp & Kelly, 2020; Hupp et al., 2019), highlighting the importance of single-shell isotope analysis to disentangle the effects of sediment mixing.

The relative abundance of symbiont-bearing foraminifera appears to have peaked at the onset of the PETM. This response varies spatially, however a general pattern is discerned as species of *Morozovella* seem to have peaked in relative abundance at low-latitudes (ODP 1209, DSDP 401), while *Acarinina* abundances peaked at high-latitudes (ODP 690) as a response to increased oligotrophy (e.g., Bralower, 2002). All locations show a strong decrease in the relative abundance of *Subbotina*, which seems to agree with impromptu observations at Site 1263. The decrease in relative abundance of *Subbotina* has also been noted for different early Eocene hyperthermals (e.g., ETM2 and H2)(Davis et al., 2022 and references therein).

4.5. Organic Carbon Burial

The rapid 30-40 kyr recovery (Bowen & Zachos, 2010; Murphy et al., 2010) suggests that increased intensified terrestrial weathering and organic carbon burial played a crucial role in the pCO_2 drawdown. Approximately 90% of organic carbon is sequestered in continental shelf and slope sediments (Hedges & Keil, 1995), and most studies agree that these regions experience increased burial of organic carbon during the PETM (e.g., Dunkley Jones et al., 2018; C. M. John et al., 2008b; Papadomanolaki et al., 2022), as increased silicate weathering and runoff likely boosted nutrient supply to shelves, enhancing productivity and prompting organic carbon preservation under anoxic conditions. Open ocean sites generally do not show signs of drastic changes in C_{org} burial, oxygen concentration, and primary productivity when compared to continental margins, restricted basins and high latitudes (Papadomanolaki et al., 2022; and references therein), causing a decline in organic carbon burial efficiency due to low organic matter fluxes under mostly oxic bottom water conditions. This decrease in C_{org} burial in the open ocean was likely met with a shift in C burial towards continental shelf environments. Hence, reduced biological pump efficiency and C_{org} burial in open oceans likely had minimal impact on sustained high atmospheric pCO_2-levels during the PETM and recovery thereof, as most carbon sequestration occurred on the continental shelf.

4.6. Current Theory and Implications

At present, the hypothesis of a breakdown in the efficiency of the marine biological pump, and concomitant decrease in photosymbiont associations is favored. The hypothesis of a decrease in thermocline strength and stratification (*hypothesis 1*) is currently not supported as the general consensus suggests an increase in oligotrophy and stratification during the PETM. Additionally, this theory fails to explain the change in the variability of $\delta^{13}C$ and $\delta^{18}O$ with size as recorded in the symbiotic and asymbiotic taxa. The alternative hypothesis suggesting an increase in depth habitat by photosymbiont-bearing planktic foraminifera (*hypothesis 2*) is not supported by this study, given the

persistence of photosymbiotic $\delta^{13}C$-size enrichment in symbiotic species during the PETM. Additionally, hypothesis 2 fails to account for the less pronounced $\delta^{13}C$ excursion observed in *Subbotina* and its development of a $\delta^{18}O$-size gradient. Instead, it is proposed that the reductions in the interspecies $\delta^{13}C$- and $\delta^{18}O$-gradients and the development of a $\delta^{18}O$-size gradient recorded in *Subbotina* resulted from the upward migration of *Subbotina* as an adaptive response to a decline in export production and increased twilight zone oligotrophy. Simultaneously, *Morozovella* and *Acarinina* are suggested to have inhabited a more constrained depth habitat as an adaptive response to the shallowing of the mixed layer and remineralization depth.

The current theory suggests that the efficiency of the marine biological pump was strongly reduced during the PETM as a consequence of the shallower and more efficient remineralization of organic matter, effectively reducing the organic matter and nutrient supply to the *twilight zone* and benthos. These findings are in line with carbon cycle modeling of the marine biological carbon pump during the Eocene hyperthermals (Griffith et al., 2021). Additionally, the findings of this study indicate a moderate decrease in the strength of photosymbiont enrichments (i.e., photosymbiont activity) during the PETM as a result of extreme environmental conditions in the surface oceans. The importance of photosymbiont associations to the foraminifer's metabolism may have fluctuated over time and/or throughout ontogeny and showed to exhibit strong spatial variation during the PETM.

This study offers a compelling case highlighting the relative resilience of photosymbiont-bearing planktic foraminifera to PETM perturbations, especially when contrasted with their asymbiotic counterparts. The widely observed phenomenon of a decrease in the relative abundance of *Subbotina* and increased abundance of photosymbiont-bearing taxa highlights the resilience and importance of sustained symbiont associations during warming episodes such as the PETM.

Estimates of the modern rate of climate change exceed that of the PETM by approximately an order of magnitude. Meanwhile, the newfound vulnerability of the marine biological carbon pump underscores the urgency of understanding the anthropogenic stresses imposed on marine ecosystems. This study highlights the importance and vulnerability of twilight zone and benthic ecosystems to reduced biological carbon pump efficiency during periods of rapid warming. Despite evidence of foraminiferal adaptive resilience to climate perturbations during the PETM, it remains uncertain how these organisms would fare under the trajectory of the current rate of climate change.

4.7. Recommendations for Future Research

The response in photosymbiont associations is spatially variable. Hence, I would like to highlight the importance of studying the response of photosymbiosis across various sites and ocean systems. Additionally, I recommend that a varied array of intervals of climate change (e.g., hyperthermals, glacials) be studied to disentangle photosymbiont response from foraminiferal test signals and assess the resilience of photosymbiont associations to climate change.

Moreover, variations in photosymbiont associations have the potential to affect variations recorded in carbon, oxygen, and boron isotopes, thereby complicating interpretations of warming, carbon cycle dynamics, ocean acidification, and pCO_2-levels during these critical intervals. Hence, I recommend the evaluation of boron isotopes (i.e., $\delta^{11}B$) in addition to the customary carbon and oxygen stable isotope analysis across different size fractions for the PETM.

Furthermore, it is recommended that single-shell stable isotope analysis be conducted spanning the onset of the PETM to capture the response of planktic foraminifera and disentangle any influence of sediment mixing across the onset of the CIE at Site 1263. It is suggested that these measurements be performed within restricted size fractions to evaluate the photosymbiotic response at the onset of the PETM. Moreover, it is suggested to conduct an abundance study at Site 1263 to compare with the other locations referenced in this paper, reflecting the spatial variation in the resilience and adaptive response of planktic foraminifera to PETM associated warming.

CONCLUSIONS

Planktic foraminiferal stable isotope records from the South Atlantic (Walvis Ridge; ODP Site 1263) provide evidence for the reduced efficiency of the marine biological carbon pump as a response to PETM warming. This study supports the idea that the remineralization of organic carbon occurred shallower and more efficiently during the PETM, effectively depleting the twilight zone and benthos of nutrients and organic matter. Moreover, this study provides support for the resilience of photosymbiont associations in planktic foraminifera to PETM warming and environmental change. It is suggested that photosymbiont associations remained relevant to these taxa and likely contributed to their survival and flourishing during the PETM. Instead, due to the implications of reduced export production and nutrient supply with depth, this study suggests that twilight zone dwelling taxa, such as *Subbotina Patagonica*, pose less resilient and more affected by extreme warming intervals such as the PETM.

These findings have critical implications for the future of anthropogenic warming and carbon emissions. The research highlights the importance and vulnerability of twilight zone and benthic ecosystems to reduced biological carbon pump efficiency during periods of rapid warming. Movement towards PETM like conditions may induce profound consequences for the efficiency of the BCP at sequestering anthropogenic carbon, twilight zone ecology and marine biological activity. The implications of which have the potential to reach far beyond the scope of Paleocene-Eocene perturbations.

ACKNOWLEDGMENTS

Firstly, I would like to thank Jim Zachos for graciously welcoming me into his lab group and providing the opportunity to delve into this ongoing, state-of-the-art research project. I would like to thank Appy Sluijs for assisting me in my endeavors of performing my master's thesis in Santa Cruz. I would further like to extend my gratitude to Eric Tappa at the University of South Caroline for technical support. Daniel Gaskell deserves my sincere appreciation for his assistance during my graduate studies, and whose insights, collaboration and discussions have significantly enriched this work. I am further grateful to Xiaodong Daisy Zhang, for her laboratory guidance and expertise.

I would like to express my gratitude to my friends at home for keeping me entertained with a well-timed call during my hours of picking foraminifera. Likewise, I would like to thank my friends in Santa Cruz for rushing me out of the lab and office on time every day for a quick dip in the ocean, fun trail run, or beautiful sunset session. Lastly, I owe a debt of gratitude to my beloved dogs, Eevee and Bella, whose comforting presence, unconditional love, and nature walks have brought joy to my days, especially during the final moments of thesis writing.

REFERENCES

Allen, A. P., Gillooly, J. F., & Brown, J. H. (2005). Linking the global carbon cycle to individual metabolism. *Functional Ecology*, *19*(2), 202–213. https://doi.org/10.1111/j.1365-2435.2005.00952.x

Aze, T., Ezard, T. H. G., Purvis, A., Coxall, H. K., Stewart, D. R. M., Wade, B. S., & Pearson, P. N. (2011). A phylogeny of Cenozoic macroperforate planktonic foraminifera from fossil data. *Biological Reviews*, *86*(4), 900–927. https://doi.org/10.1111/j.1469-185X.2011.00178.x

Aze, T., Pearson, P. N., Dickson, A. J., Badger, M. P. S., Bown, P. R., Pancost, R. D., Gibbs, S. J., Huber, B. T., Leng, M. J., Coe, A. L., Cohen, A. S., & Foster, G. L. (2014). Extreme warming of tropical waters during the Paleocene–Eocene Thermal Maximum. *Geology*, *42*(9), 739–742. https://doi.org/10.1130/G35637.1

Babila, T. L., Penman, D. E., Hönisch, B., Kelly, D. C., Bralower, T. J., Rosenthal, Y., & Zachos, J. C. (2018). Capturing the global signature of surface ocean acidification during the Palaeocene–Eocene Thermal Maximum. *Philosophical Transactions of the Royal Society A: Mathematical, Physical and Engineering Sciences*, *376*(2130), 20170072. https://doi.org/10.1098/rsta.2017.0072

Babila, T. L., Rosenthal, Y., Wright, J. D., & Miller, K. G. (2016). A continental shelf perspective of ocean acidification and temperature evolution during the Paleocene-Eocene Thermal Maximum. *Geology*, *44*(4), 275–278. https://doi.org/10.1130/G37522.1

Bains, S., Norris, R. D., Corfield, R. M., & Faul, K. L. (2000). Termination of global warmth at the Palaeocene/Eocene boundary through productivity feedback. *Nature*, *407*(6801), Article 6801. https://doi.org/10.1038/35025035

Barrett, R., Adebowale, M., Birch, H., Wilson, J. D., & Schmidt, D. N. (2023). Planktic Foraminiferal Resilience to Environmental Change Associated With the PETM. *Paleoceanography and Paleoclimatology*, *38*(8), e2022PA004534. https://doi.org/10.1029/2022PA004534

Bé, A. W. H., Spero, H. J., & Anderson, O. R. (1982). Effects of symbiont elimination and reinfection on the life processes of the planktonic foraminifer Globigerinoides sacculifer. *Marine Biology*, *70*(1), 73–86. https://doi.org/10.1007/BF00397298

Berger, W. H., Killingley J.S., & Vincent E. (1978). Stable Isotopes In Deep-Sea Carbonates: Box Core Erdc-92, West Equatorial Pacific. *Stable Isotopes In Deep-Sea Carbonates: Box Core Erdc-92, West Equatorial Pacific.*

Berggren, W. A., & Norris, R. D. (1997). Biostratigraphy, Phylogeny and Systematics of Paleocene Trochospiral Planktic Foraminifera. *Micropaleontology*, *43*, i–116. https://doi.org/10.2307/1485988

Berndt, C., Planke, S., Alvarez Zarikian, C. A., Frieling, J., Jones, M. T., Millett, J. M., Brinkhuis, H., Bünz, S., Svensen, H. H., Longman, J., Scherer, R. P., Karstens, J., Manton, B., Nelissen, M., Reed, B., Faleide, J. I., Huismans, R. S., Agarwal, A., Andrews, G. D. M., … Yager, S. L. (2023). Shallow-water hydrothermal venting linked to the Palaeocene–Eocene Thermal Maximum. *Nature Geoscience*, *16*(9), Article 9. https://doi.org/10.1038/s41561-023-01246-8

Bice, K. L., & Marotzke, J. (2002). Could changing ocean circulation have destabilized methane hydrate at the Paleocene/Eocene boundary? *Paleoceanography*, *17*(2), 8-1-8–12. https://doi.org/10.1029/2001PA000678

Bijma, J., Spero, H. J., & Lea, D. W. (1999). Reassessing Foraminiferal Stable Isotope Geochemistry: Impact of the Oceanic Carbonate System (Experimental Results). In G. Fischer & G. Wefer (Eds.), *Use of Proxies in Paleoceanography: Examples from the South Atlantic* (pp. 489–512). Springer. https://doi.org/10.1007/978-3-642-58646-0_20

Bindoff, N., Cheung, W., Kairo, J. G., Aristegui, J., Guinder, V., Hallberg, R., Hilmi, N., Jiao, N., Karim, M., Levin, L., O'Donoghue, S. H., Purca, S., Rinkevich, B., Suga, T., Tagliabue, A., Williamson, P., Acar, S.,

Alava, J. J., Allison, E., & Whalen, C. (2019). *Changing Ocean, Marine Ecosystems, and Dependent Communities (09 SROCC Ch05 FINAL-1)* (pp. 447–588).

Birch, H., Coxall, H. K., Pearson, P. N., Kroon, D., & O'Regan, M. (2013). Planktonic foraminifera stable isotopes and water column structure: Disentangling ecological signals. *Marine Micropaleontology*, *101*, 127–145. https://doi.org/10.1016/j.marmicro.2013.02.002

Boscolo-Galazzo, F., Crichton, K. A., Barker, S., & Pearson, P. N. (2018). Temperature dependency of metabolic rates in the upper ocean: A positive feedback to global climate change? *Global and Planetary Change*, *170*, 201–212. https://doi.org/10.1016/j.gloplacha.2018.08.017

Boscolo-Galazzo, F., Crichton, K. A., Ridgwell, A., Mawbey, E. M., Wade, B. S., & Pearson, P. N. (2021). Temperature controls carbon cycling and biological evolution in the ocean twilight zone. *Science*, *371*(6534), 1148–1152. https://doi.org/10.1126/science.abb6643

Bowen, G. J., Beerling, D. J., Koch, P. L., Zachos, J. C., & Quattlebaum, T. (2004). A humid climate state during the Palaeocene/Eocene thermal maximum. *Nature*, *432*(7016), Article 7016. https://doi.org/10.1038/nature03115

Bowen, G. J., & Zachos, J. C. (2010). Rapid carbon sequestration at the termination of the Palaeocene–Eocene Thermal Maximum. *Nature Geoscience*, *3*(12), 866–869. https://doi.org/10.1038/ngeo1014

Bralower, T. J. (2002). Evidence of surface water oligotrophy during the Paleocene-Eocene thermal maximum: Nannofossil assemblage data from Ocean Drilling Program Site 690, Maud Rise, Weddell Sea. *Paleoceanography*, *17*(2), 13-1-13–12. https://doi.org/10.1029/2001PA000662

Brault, M.-O., Matthews, H. D., & Mysak, L. A. (2017). The importance of terrestrial weathering changes in multimillennial recovery of the global carbon cycle: A two-dimensional perspective. *Earth System Dynamics*, *8*(2), 455–475. https://doi.org/10.5194/esd-8-455-2017

Buesseler, K. O. (1998). The decoupling of production and particulate export in the surface ocean. *Global Biogeochemical Cycles*, *12*(2), 297–310. https://doi.org/10.1029/97GB03366

Canadell, J. G., Monteiro, P. M. S., Costa, M. H., Cunha, L. C. D., Cox, P. M., Eliseev, A. V., Henson, S., Ishii, M., Jaccard, S., Koven, C., Lohila, A., Patra, P. K., Piao, S., Syampungani, S., Zaehle, S., Zickfeld, K., Alexandrov, G. A., Bala, G., Bopp, L., … Lebehot, A. D. (2021). Global Carbon and other Biogeochemical Cycles and Feedbacks. In *IPCC AR6 WGI, Final Government Distribution* (p. chapter 5). https://hal.science/hal-03336145

Carmichael, M. J., Inglis, G. N., Badger, M. P. S., Naafs, B. D. A., Behrooz, L., Remmelzwaal, S., Monteiro, F. M., Rohrssen, M., Farnsworth, A., Buss, H. L., Dickson, A. J., Valdes, P. J., Lunt, D. J., & Pancost, R. D. (2017). Hydrological and associated biogeochemical consequences of rapid global warming during the Paleocene-Eocene Thermal Maximum. *Global and Planetary Change*, *157*, 114–138. https://doi.org/10.1016/j.gloplacha.2017.07.014

Colosimo, A. B., Bralower, T. J., & Zachos, J. C. (2005). Evidence for lysocline shoaling at the Paleocene/Eocene Thermal Maximum on Shatsky Rise, northwest Pacific. *Proceedings of the Ocean Drilling Program: Scientific Results*, *198*. http://www.scopus.com/inward/record.url?scp=45449117049&partnerID=8YFLogxK

Cossins, A. R., & Bowler, K. (1987). *Temperature biology of animals*. Chapman and Hall.

Coxall, H. K., Pearson, P. N., Wilson, P. A., & Sexton, P. F. (2007). Iterative evolution of digitate planktonic foraminifera. *Paleobiology*, *33*(4), 495–516. https://doi.org/10.1666/06034.1

Crichton, K. A., Wilson, J. D., Ridgwell, A., Boscolo-Galazzo, F., John, E. H., Wade, B. S., & Pearson, P. N. (2023). What the geological past can tell us about the future of the ocean's twilight zone. *Nature Communications*, *14*(1), Article 1. https://doi.org/10.1038/s41467-023-37781-6

Crouch, E. M., Heilmann-Clausen, C., Brinkhuis, H., Morgans, H. E. G., Rogers, K. M., Egger, H., & Schmitz, B. (2001). Global dinoflagellate event associated with the late Paleocene thermal

maximum. *Geology*, *29*(4), 315–318. https://doi.org/10.1130/0091-7613(2001)029<0315:GDEAWT>2.0.CO;2

Cui, Y., Kump, L. R., Ridgwell, A. J., Charles, A. J., Junium, C. K., Diefendorf, A. F., Freeman, K. H., Urban, N. M., & Harding, I. C. (2011). Slow release of fossil carbon during the Palaeocene–Eocene Thermal Maximum. *Nature Geoscience*, *4*(7), Article 7. https://doi.org/10.1038/ngeo1179

Davis, C. V., Shaw, J. O., D'haenens, S., Thomas, E., & Hull, P. M. (2022). Photosymbiont associations persisted in planktic foraminifera during early Eocene hyperthermals at Shatsky Rise (Pacific Ocean). *PLOS ONE*, *17*(9), e0267636. https://doi.org/10.1371/journal.pone.0267636

DeConto, R. M., Galeotti, S., Pagani, M., Tracy, D., Schaefer, K., Zhang, T., Pollard, D., & Beerling, D. J. (2012). Past extreme warming events linked to massive carbon release from thawing permafrost. *Nature*, *484*(7392), Article 7392. https://doi.org/10.1038/nature10929

D'Hondt, S., & Zachos, J. C. (1993). On stable isotopic variation and earliest Paleocene planktonic foraminifera. *Paleoceanography*, *8*(4), 527–547. https://doi.org/10.1029/93PA00952

D'Hondt, S., Zachos, J. C., & Schultz, G. (1994). Stable isotopic signals and photosymbiosis in Late Paleocene planktic foraminifera. *Paleobiology*, *20*(3), 391–406. https://doi.org/10.1017/S0094837300012847

Dickens, G. R., Castillo, M. M., & Walker, J. C. G. (1997). A blast of gas in the latest Paleocene: Simulating first-order effects of massive dissociation of oceanic methane hydrate. *Geology*, *25*(3), 259–262. https://doi.org/10.1130/0091-7613(1997)025<0259:ABOGIT>2.3.CO;2

Dickens, G. R., O'Niel, J., Rea, D., & Owen, R. (1995). Dissociation of oceanic methane hydrate as a cause of the carbon isotope excursion at the end of the Paleocene. *Paleoceanography*, *10*, 965–971. https://doi.org/10.1029/95PA02087

Dunkley Jones, T., Lunt, D. J., Schmidt, D. N., Ridgwell, A., Sluijs, A., Valdes, P. J., & Maslin, M. (2013). Climate model and proxy data constraints on ocean warming across the Paleocene–Eocene Thermal Maximum. *Earth-Science Reviews*, *125*, 123–145. https://doi.org/10.1016/j.earscirev.2013.07.004

Dunkley Jones, T., Manners, H. R., Hoggett, M., Kirtland Turner, S., Westerhold, T., Leng, M. J., Pancost, R. D., Ridgwell, A., Alegret, L., Duller, R., & Grimes, S. T. (2018). Dynamics of sediment flux to a bathyal continental margin section through the Paleocene–Eocene Thermal Maximum. *Climate of the Past*, *14*(7), 1035–1049. https://doi.org/10.5194/cp-14-1035-2018

Frieling, J., Gebhardt, H., Huber, M., Adekeye, O. A., Akande, S. O., Reichart, G.-J., Middelburg, J. J., Schouten, S., & Sluijs, A. (2017a). Extreme warmth and heat-stressed plankton in the tropics during the Paleocene-Eocene Thermal Maximum. *Science Advances*, *3*(3), e1600891. https://doi.org/10.1126/sciadv.1600891

Frieling, J., Gebhardt, H., Huber, M., Adekeye, O. A., Akande, S. O., Reichart, G.-J., Middelburg, J. J., Schouten, S., & Sluijs, A. (2017b). Extreme warmth and heat-stressed plankton in the tropics during the Paleocene-Eocene Thermal Maximum. *Science Advances*, *3*(3), e1600891. https://doi.org/10.1126/sciadv.1600891

Frieling, J., Peterse, F., Lunt, D. J., Bohaty, S. M., Sinninghe Damsté, J. S., Reichart, G.-J., & Sluijs, A. (2019). Widespread Warming Before and Elevated Barium Burial During the Paleocene-Eocene Thermal Maximum: Evidence for Methane Hydrate Release? *Paleoceanography and Paleoclimatology*, *34*(4), 546–566. https://doi.org/10.1029/2018PA003425

Frieling, J., Reichart, G.-J., Middelburg, J. J., Röhl, U., Westerhold, T., Bohaty, S. M., & Sluijs, A. (2018). Tropical Atlantic climate and ecosystem regime shifts during the Paleocene–Eocene Thermal Maximum. *Climate of the Past*, *14*(1), 39–55. https://doi.org/10.5194/cp-14-39-2018

Frieling, J., Svensen, H. H., Planke, S., Cramwinckel, M. J., Selnes, H., & Sluijs, A. (2016). Thermogenic methane release as a cause for the long duration of the PETM. *Proceedings of the National Academy of Sciences*, *113*(43), 12059–12064. https://doi.org/10.1073/pnas.1603348113

Gaskell, D. E., & Hull, P. M. (2019). Symbiont arrangement and metabolism can explain high δ13C in Eocene planktonic foraminifera. *Geology*, *47*(12), 1156–1160. https://doi.org/10.1130/G46304.1

Gibbs, S. J., Bown, P. R., Sessa, J. A., Bralower, T. J., & Wilson, P. A. (2006). Nannoplankton Extinction and Origination Across the Paleocene-Eocene Thermal Maximum. *Science*, *314*(5806), 1770–1773. https://doi.org/10.1126/science.1133902

Gibbs, S. J., Bralower, T. J., Bown, P. R., Zachos, J. C., & Bybell, L. M. (2006). Shelf and open-ocean calcareous phytoplankton assemblages across the Paleocene-Eocene Thermal Maximum: Implications for global productivity gradients. *Geology*, *34*(4), 233–236. https://doi.org/10.1130/G22381.1

Griffith, E. M., Thomas, E., Lewis, A. R., Penman, D. E., Westerhold, T., & Winguth, A. M. E. (2021). Bentho-Pelagic Decoupling: The Marine Biological Carbon Pump During Eocene Hyperthermals. *Paleoceanography and Paleoclimatology*, *36*(3), e2020PA004053. https://doi.org/10.1029/2020PA004053

Gruber, N., Clement, D., Carter, B. R., Feely, R. A., van Heuven, S., Hoppema, M., Ishii, M., Key, R. M., Kozyr, A., Lauvset, S. K., Lo Monaco, C., Mathis, J. T., Murata, A., Olsen, A., Perez, F. F., Sabine, C. L., Tanhua, T., & Wanninkhof, R. (2019). The oceanic sink for anthropogenic CO2 from 1994 to 2007. *Science*, *363*(6432), 1193–1199. https://doi.org/10.1126/science.aau5153

Gutjahr, M., Ridgwell, A., Sexton, P. F., Anagnostou, E., Pearson, P. N., Pälike, H., Norris, R. D., Thomas, E., & Foster, G. L. (2017a). Very large release of mostly volcanic carbon during the Palaeocene–Eocene Thermal Maximum. *Nature*, *548*(7669), Article 7669. https://doi.org/10.1038/nature23646

Gutjahr, M., Ridgwell, A., Sexton, P. F., Anagnostou, E., Pearson, P. N., Pälike, H., Norris, R. D., Thomas, E., & Foster, G. L. (2017b). Very large release of mostly volcanic carbon during the Palaeocene–Eocene Thermal Maximum. *Nature*, *548*(7669), Article 7669. https://doi.org/10.1038/nature23646

Handley, L., O'Halloran, A., Pearson, P. N., Hawkins, E., Nicholas, C. J., Schouten, S., McMillan, I. K., & Pancost, R. D. (2012). Changes in the hydrological cycle in tropical East Africa during the Paleocene–Eocene Thermal Maximum. *Palaeogeography, Palaeoclimatology, Palaeoecology*, *329–330*, 10–21. https://doi.org/10.1016/j.palaeo.2012.02.002

Hedges, J. I., & Keil, R. G. (1995). Sedimentary organic matter preservation: An assessment and speculative synthesis. *Marine Chemistry*, *49*(2), 81–115. https://doi.org/10.1016/0304-4203(95)00008-F

Hupp, B., & Kelly, D. C. (2020). Delays, Discrepancies, and Distortions: Size-Dependent Sediment Mixing and the Deep-Sea Record of the Paleocene-Eocene Thermal Maximum From ODP Site 690 (Weddell Sea). *Paleoceanography and Paleoclimatology*, *35*(11), e2020PA004018. https://doi.org/10.1029/2020PA004018

Hupp, B. N., Kelly, D. C., & Williams, J. W. (2022). Isotopic filtering reveals high sensitivity of planktic calcifiers to Paleocene–Eocene thermal maximum warming and acidification. *Proceedings of the National Academy of Sciences*, *119*(9), e2115561119. https://doi.org/10.1073/pnas.2115561119

Hupp, B. N., Kelly, D. C., Zachos, J. C., & Bralower, T. J. (2019). Effects of size-dependent sediment mixing on deep-sea records of the Paleocene-Eocene Thermal Maximum. *Geology*, *47*(8), 749–752. https://doi.org/10.1130/G46042.1

Jennions, S. M., Thomas, E., Schmidt, D. N., Lunt, D., & Ridgwell, A. (2015). Changes in benthic ecosystems and ocean circulation in the Southeast Atlantic across Eocene Thermal Maximum 2. *Paleoceanography*, *30*(8), 1059–1077. https://doi.org/10.1002/2015PA002821

John, C. M., Bohaty, S. M., Zachos, J. C., Sluijs, A., Gibbs, S., Brinkhuis, H., & Bralower, T. J. (2008a). North American continental margin records of the Paleocene-Eocene thermal maximum: Implications for global carbon and hydrological cycling. *Paleoceanography*, *23*(2). https://doi.org/10.1029/2007PA001465

John, C. M., Bohaty, S. M., Zachos, J. C., Sluijs, A., Gibbs, S., Brinkhuis, H., & Bralower, T. J. (2008b). North American continental margin records of the Paleocene-Eocene thermal maximum: Implications for global carbon and hydrological cycling. *Paleoceanography*, *23*(2). https://doi.org/10.1029/2007PA001465

John, E. H., Pearson, P. N., Coxall, H. K., Birch, H., Wade, B. S., & Foster, G. L. (2013). Warm ocean processes and carbon cycling in the Eocene. *Philosophical Transactions of the Royal Society A: Mathematical, Physical and Engineering Sciences*, *371*(2001), 20130099. https://doi.org/10.1098/rsta.2013.0099

Kelly, D. C., Bralower, T. J., & Zachos, J. C. (1998). Evolutionary consequences of the latest Paleocene thermal maximum for tropical planktonic foraminifera. *Palaeogeography, Palaeoclimatology, Palaeoecology*, *141*(1), 139–161. https://doi.org/10.1016/S0031-0182(98)00017-0

Kelly, D. C., Zachos, J. C., Bralower, T. J., & Schellenberg, S. A. (2005). Enhanced terrestrial weathering/runoff and surface ocean carbonate production during the recovery stages of the Paleocene-Eocene thermal maximum. *Paleoceanography*, *20*(4). https://doi.org/10.1029/2005PA001163

Kender, S., Bogus, K., Pedersen, G. K., Dybkjær, K., Mather, T. A., Mariani, E., Ridgwell, A., Riding, J. B., Wagner, T., Hesselbo, S. P., & Leng, M. J. (2021). Paleocene/Eocene carbon feedbacks triggered by volcanic activity. *Nature Communications*, *12*, 5186. https://doi.org/10.1038/s41467-021-25536-0

Kennett, J. P., & Stott, L. D. (1991). Abrupt deep-sea warming, palaeoceanographic changes and benthic extinctions at the end of the Palaeocene. *Nature*, *353*(6341), Article 6341. https://doi.org/10.1038/353225a0

Kirtland Turner, S., & Ridgwell, A. (2016). Development of a novel empirical framework for interpreting geological carbon isotope excursions, with implications for the rate of carbon injection across the PETM. *Earth and Planetary Science Letters*, *435*, 1–13. https://doi.org/10.1016/j.epsl.2015.11.027

Koch, P. L., Zachos, J. C., & Gingerich, P. D. (1992). Correlation between isotope records in marine and continental carbon reservoirs near the Palaeocene/Eocene boundary. *Nature*, *358*(6384), Article 6384. https://doi.org/10.1038/358319a0

Kurtz, A. C., Kump, L. R., Arthur, M. A., Zachos, J. C., & Paytan, A. (2003). Early Cenozoic decoupling of the global carbon and sulfur cycles. *Paleoceanography*, *18*(4). https://doi.org/10.1029/2003PA000908

Li, M., Bralower, T. J., Kump, L. R., Self-Trail, J. M., Zachos, J. C., Rush, W. D., & Robinson, M. M. (2022). Astrochronology of the Paleocene-Eocene Thermal Maximum on the Atlantic Coastal Plain. *Nature Communications*, *13*(1), Article 1. https://doi.org/10.1038/s41467-022-33390-x

Lombard, F., Erez, J., Michel, E., & Labeyrie, L. (2009). Temperature effect on respiration and photosynthesis of the symbiont-bearing planktonic foraminifera Globigerinoides ruber, Orbulina universa, and Globigerinella siphonifera. *Limnology and Oceanography*, *54*(1), 210–218. https://doi.org/10.4319/lo.2009.54.1.0210

Lourens, L. J., Sluijs, A., Kroon, D., Zachos, J. C., Thomas, E., Röhl, U., Bowles, J., & Raffi, I. (2005). Astronomical pacing of late Palaeocene to early Eocene global warming events. *Nature*, *435*(7045), Article 7045. https://doi.org/10.1038/nature03814

Lunt, D. J., Valdes, P. J., Jones, T. D., Ridgwell, A., Haywood, A. M., Schmidt, D. N., Marsh, R., & Maslin, M. (2010). CO2-driven ocean circulation changes as an amplifier of Paleocene-Eocene thermal maximum hydrate destabilization. *Geology*, *38*(10), 875–878. https://doi.org/10.1130/G31184.1

Ma, Z., Gray, E., Thomas, E., Murphy, B., Zachos, J., & Paytan, A. (2014). Carbon sequestration during the Palaeocene–Eocene Thermal Maximum by an efficient biological pump. *Nature Geoscience*, *7*(5), Article 5. https://doi.org/10.1038/ngeo2139

Makarova, M., Wright, J. D., Miller, K. G., Babila, T. L., Rosenthal, Y., & Park, J. I. (2017). Hydrographic and ecologic implications of foraminiferal stable isotopic response across the U.S. mid-Atlantic continental shelf during the Paleocene-Eocene Thermal Maximum. *Paleoceanography*, *32*(1), 56–73. https://doi.org/10.1002/2016PA002985

Matsui, H., Nishi, H., Takashima, R., Kuroyanagi, A., Ikehara, M., Takayanagi, H., & Iryu, Y. (2016). Changes in the depth habitat of the Oligocene planktic foraminifera (Dentoglobigerina venezuelana) induced by thermocline deepening in the eastern equatorial Pacific. *Paleoceanography*, *31*(6), 715–731. https://doi.org/10.1002/2016PA002950

McCarren, H., Thomas, E., Hasegawa, T., Röhl, U., & Zachos, J. C. (2008). Depth dependency of the Paleocene-Eocene carbon isotope excursion: Paired benthic and terrestrial biomarker records (Ocean Drilling Program Leg 208, Walvis Ridge). *Geochemistry, Geophysics, Geosystems*, *9*(10). https://doi.org/10.1029/2008GC002116

McInerney, F. A., & Wing, S. L. (2011). The Paleocene-Eocene Thermal Maximum: A Perturbation of Carbon Cycle, Climate, and Biosphere with Implications for the Future. *Annual Review of Earth and Planetary Sciences*, *39*(1), 489–516. https://doi.org/10.1146/annurev-earth-040610-133431

Mendes, P. A. de J., & Thomsen, L. (2012). Effects of Ocean Acidification on the Ballast of Surface Aggregates Sinking through the Twilight Zone. *PLOS ONE*, *7*(12), e50865. https://doi.org/10.1371/journal.pone.0050865

Moretti, S., Auderset, A., Deutsch, C., Schmitz, R., Gerber, L., Thomas, E., Luciani, V., Petrizzo, M. R., Schiebel, R., Tripati, A., Sexton, P., Norris, R., D'Onofrio, R., Zachos, J., Sigman, D. M., Haug, G. H., & Martínez-García, A. (2024). Oxygen rise in the tropical upper ocean during the Paleocene-Eocene Thermal Maximum. *Science*, *383*(6684), 727–731. https://doi.org/10.1126/science.adh4893

Murphy, B. H., Farley, K. A., & Zachos, J. C. (2010). An extraterrestrial 3He-based timescale for the Paleocene–Eocene thermal maximum (PETM) from Walvis Ridge, IODP Site 1266. *Geochimica et Cosmochimica Acta*, *74*(17), 5098–5108. https://doi.org/10.1016/j.gca.2010.03.039

Nowicki, M., DeVries, T., & Siegel, D. A. (2022). Quantifying the Carbon Export and Sequestration Pathways of the Ocean's Biological Carbon Pump. *Global Biogeochemical Cycles*, *36*(3), e2021GB007083. https://doi.org/10.1029/2021GB007083

Nunes, F., & Norris, R. D. (2006). Abrupt reversal in ocean overturning during the Palaeocene/Eocene warm period. *Nature*, *439*(7072), 60–63. https://doi.org/10.1038/nature04386

Nwojiji, C., Marret, F., Caswell, B., Okoro, A. U., & Igwe, E. O. (2023). Benthic foraminiferal turnover and trait changes across the Palaeocene–Eocene Thermal Maximum (PETM) at ODP site 1265A, Walvis Ridge, SE Atlantic Ocean. *Arabian Journal of Geosciences*, *16*(5), 324. https://doi.org/10.1007/s12517-023-11417-x

Olivarez Lyle, A., & Lyle, M. W. (2006). Missing organic carbon in Eocene marine sediments: Is metabolism the biological feedback that maintains end-member climates? *Paleoceanography*, *21*(2). https://doi.org/10.1029/2005PA001230

Pagani, M., Pedentchouk, N., Huber, M., Sluijs, A., Schouten, S., Brinkhuis, H., Sinninghe Damsté, J. S., & Dickens, G. R. (2006). Arctic hydrology during global warming at the Palaeocene/Eocene thermal maximum. *Nature*, *442*(7103), 671–675. https://doi.org/10.1038/nature05043

Papadomanolaki, N. M., Sluijs, A., & Slomp, C. P. (2022). Eutrophication and Deoxygenation Forcing of Marginal Marine Organic Carbon Burial During the PETM. *Paleoceanography and Paleoclimatology*, *37*(3), e2021PA004232. https://doi.org/10.1029/2021PA004232

Pardo, A., Keller, G., Molina, E., & Canudo, JoséI. (1997). Planktic foraminiferal turnover across the Paleocene-Eocene transition at DSDP Site 401, Bay of Biscay, North Atlantic. *Marine Micropaleontology*, *29*(2), 129–158. https://doi.org/10.1016/S0377-8398(96)00035-7

Pearson, P. N., Olsson, R. K., Huber, B. T., Hemleben, C., & Berggren, W. A. (2006). *Atlas of eocene planktonic foraminifera* (P. N. Pearson, R. K. Olsson, B. T. Huber, C. Hemleben, & W. A. Berggren, Eds.; 41; Issue 41). Cushman Foundation for Foraminiferal Research. https://orca.cardiff.ac.uk/id/eprint/15234/

Penman, D. E. (2016). Silicate weathering and North Atlantic silica burial during the Paleocene-Eocene Thermal Maximum. *Geology*, *44*(9), 731–734. https://doi.org/10.1130/G37704.1

Penman, D. E., Hönisch, B., Zeebe, R. E., Thomas, E., & Zachos, J. C. (2014). Rapid and sustained surface ocean acidification during the Paleocene-Eocene Thermal Maximum. *Paleoceanography*, *29*(5), 357–369. https://doi.org/10.1002/2014PA002621

Petrizzo, M. R. (2007). The onset of the Paleocene–Eocene Thermal Maximum (PETM) at Sites 1209 and 1210 (Shatsky Rise, Pacific Ocean) as recorded by planktonic foraminifera. *Marine Micropaleontology*, *63*(3), 187–200. https://doi.org/10.1016/j.marmicro.2006.11.007

Piedrahita, V. A., Galeotti, S., Zhao, X., Roberts, A. P., Rohling, E. J., Heslop, D., Florindo, F., Grant, K. M., Rodríguez-Sanz, L., Reghellin, D., & Zeebe, R. E. (2022). Orbital phasing of the Paleocene-Eocene Thermal Maximum. *Earth and Planetary Science Letters*, *598*, 117839. https://doi.org/10.1016/j.epsl.2022.117839

Ravelo, A. C., & Fairbanks, R. G. (1995). Carbon isotopic fractionation in multiple species of planktonic foraminifera from core-tops in the tropical Atlantic. *Oceanographic Literature Review*, *10*(42), 854.

Röhl, U., Westerhold, T., Bralower, T. J., & Zachos, J. C. (2007). On the duration of the Paleocene-Eocene thermal maximum (PETM). *Geochemistry, Geophysics, Geosystems*, *8*(12). https://doi.org/10.1029/2007GC001784

Scheibner, C., Speijer, R. P., & Marzouk, A. M. (2005). Turnover of larger foraminifera during the Paleocene-Eocene Thermal Maximum and paleoclimatic control on the evolution of platform ecosystems. *Geology*, *33*(6), 493–496. https://doi.org/10.1130/G21237.1

Schmitz, B., & Pujalte, V. (2007). Abrupt increase in seasonal extreme precipitation at the Paleocene-Eocene boundary. *Geology*, *35*(3), 215–218. https://doi.org/10.1130/G23261A.1

Schneider, L. J., Bralower, T. J., Kump, L. R., & Patzkowsky, M. E. (2013). Calcareous nannoplankton ecology and community change across the Paleocene-Eocene Thermal Maximum. *Paleobiology*, *39*(4), 628–647. https://doi.org/10.1666/12050

Schoon, P. L., Heilmann-Clausen, C., Schultz, B. P., Sinninghe Damsté, J. S., & Schouten, S. (2015). Warming and environmental changes in the eastern North Sea Basin during the Palaeocene–Eocene Thermal Maximum as revealed by biomarker lipids. *Organic Geochemistry*, *78*, 79–88. https://doi.org/10.1016/j.orggeochem.2014.11.003

Shaw, J. O., D'haenens, S., Thomas, E., Norris, R. D., Lyman, J. A., Bornemann, A., & Hull, P. M. (2021). Photosymbiosis in planktonic foraminifera across the Paleocene–Eocene thermal maximum. *Paleobiology*, *47*(4), 632–647. https://doi.org/10.1017/pab.2021.7

Si, W., & Aubry, M.-P. (2018). Vital Effects and Ecologic Adaptation of Photosymbiont-Bearing Planktonic Foraminifera During the Paleocene-Eocene Thermal Maximum, Implications for Paleoclimate. *Paleoceanography and Paleoclimatology*, *33*(1), 112–125. https://doi.org/10.1002/2017PA003219

Sluijs, A., Bijl, P. K., Schouten, S., Röhl, U., Reichart, G.-J., & Brinkhuis, H. (2011). Southern ocean warming, sea level and hydrological change during the Paleocene-Eocene thermal maximum. *Climate of the Past*, *7*(1), 47–61. https://doi.org/10.5194/cp-7-47-2011

Sluijs, A., Bowen, G. J., Brinkhuis, H., Lourens, L. J., & Thomas, E. (2007). The Palaeocene–Eocene Thermal Maximum super greenhouse: Biotic and geochemical signatures, age models and

mechanisms of global change. In M. Williams, A. M. Haywood, F. J. Gregory, & D. N. Schmidt (Eds.), *Deep-Time Perspectives on Climate Change: Marrying the Signal from Computer Models and Biological Proxies* (Vol. 2, p. 0). Geological Society of London. https://doi.org/10.1144/TMS002.15

Sluijs, A., Brinkhuis, H., Schouten, S., Bohaty, S. M., John, C. M., Zachos, J. C., Reichart, G.-J., Sinninghe Damsté, J. S., Crouch, E. M., & Dickens, G. R. (2007). Environmental precursors to rapid light carbon injection at the Palaeocene/Eocene boundary. *Nature*, *450*(7173), Article 7173. https://doi.org/10.1038/nature06400

Sluijs, A., Schouten, S., Pagani, M., Woltering, M., Brinkhuis, H., Damsté, J. S. S., Dickens, G. R., Huber, M., Reichart, G.-J., Stein, R., Matthiessen, J., Lourens, L. J., Pedentchouk, N., Backman, J., & Moran, K. (2006). Subtropical Arctic Ocean temperatures during the Palaeocene/Eocene thermal maximum. *Nature*, *441*(7093), 610–613. https://doi.org/10.1038/nature04668

Sluijs, A., van Roij, L., Harrington, G. J., Schouten, S., Sessa, J. A., LeVay, L. J., Reichart, G.-J., & Slomp, C. P. (2014). Warming, euxinia and sea level rise during the Paleocene–Eocene Thermal Maximum on the Gulf Coastal Plain: Implications for ocean oxygenation and nutrient cycling. *Climate of the Past*, *10*(4), 1421–1439. https://doi.org/10.5194/cp-10-1421-2014

Speijer, R., Scheibner, C., Stassen, P., & Morsi, A.-M. M. (2012). Response of marine ecosystems to deep-time global warming: A synthesis of biotic patterns across the Paleocene-Eocene thermal maximum (PETM). *Austrian Journal of Earth Sciences*, *105*(1), 6–16.

Spero, H. J., Bijma, J., Lea, D. W., & Bemis, B. E. (1997). Effect of seawater carbonate concentration on foraminiferal carbon and oxygen isotopes. *Nature*, *390*(6659), Article 6659. https://doi.org/10.1038/37333

Spero, H. J., & DeNiro, M. J. (1987). The influence of symbiont photosynthesis on the δ18O and δ13C values of planktonic foraminiferal shell calcite. *Symbiosis (Philadelphia, PA)*, *4*(1–3), 213–228.

Spero, H. J., & Lea, D. W. (1993). Intraspecific stable isotope variability in the planktic foraminifera Globigerinoides sacculifer: Results from laboratory experiments. *Marine Micropaleontology*, *22*(3), 221–234. https://doi.org/10.1016/0377-8398(93)90045-Y

Spero, H. J., Lerche, I., & Williams, D. F. (1991). Opening the carbon isotope "vital effect" black box, 2, Quantitative model for interpreting foraminiferal carbon isotope data. *Paleoceanography*, *6*(6), 639–655. https://doi.org/10.1029/91PA02022

Spero, H. J., & Parker, S. L. (1985). Photosynthesis in the symbiotic planktonic foraminifer Orbulina universa, and its potential contribution to oceanic primary productivity. *Journal of Foraminiferal Research*, *15*(4), 273–281. https://doi.org/10.2113/gsjfr.15.4.273

Spero, H. J., & Williams, D. F. (1988). Extracting environmental information from planktonic foraminiferal δ13C data. *Nature*, *335*(6192), Article 6192. https://doi.org/10.1038/335717a0

Stoll, H. M., Shimizu, N., Archer, D., & Ziveri, P. (2007). Coccolithophore productivity response to greenhouse event of the Paleocene–Eocene Thermal Maximum. *Earth and Planetary Science Letters*, *258*(1), 192–206. https://doi.org/10.1016/j.epsl.2007.03.037

Storey, M., Duncan, R. A., & Swisher, C. C. (2007). Paleocene-Eocene Thermal Maximum and the Opening of the Northeast Atlantic. *Science*, *316*(5824), 587–589. https://doi.org/10.1126/science.1135274

Svensen, H., Planke, S., & Corfu, F. (2010). Zircon dating ties NE Atlantic sill emplacement to initial Eocene global warming. *Journal of the Geological Society*, *167*(3), 433–436. https://doi.org/10.1144/0016-76492009-125

Svensen, H., Planke, S., Malthe-Sørenssen, A., Jamtveit, B., Myklebust, R., Rasmussen Eidem, T., & Rey, S. S. (2004). Release of methane from a volcanic basin as a mechanism for initial Eocene global warming. *Nature*, *429*(6991), Article 6991. https://doi.org/10.1038/nature02566

Sweetman, A. K., Thurber, A. R., Smith, C. R., Levin, L. A., Mora, C., Wei, C.-L., Gooday, A. J., Jones, D. O. B., Rex, M., Yasuhara, M., Ingels, J., Ruhl, H. A., Frieder, C. A., Danovaro, R., Würzberg, L., Baco, A., Grupe, B. M., Pasulka, A., Meyer, K. S., … Roberts, J. M. (2017). Major impacts of climate change on deep-sea benthic ecosystems. *Elementa: Science of the Anthropocene*, *5*, 4. https://doi.org/10.1525/elementa.203

Thomas, D. J., Zachos, J. C., Bralower, T. J., Thomas, E., & Bohaty, S. (2002). Warming the fuel for the fire: Evidence for the thermal dissociation of methane hydrate during the Paleocene-Eocene thermal maximum. *Geology*, *30*(12), 1067–1070. https://doi.org/10.1130/0091-7613(2002)030<1067:WTFFTF>2.0.CO;2

Thomas, E. (2007). Cenozoic mass extinctions in the deep sea: What perturbs the largest habitat on Earth? In S. Monechi, R. Coccioni, & M. Rampino (Eds.), *Large Ecosystem Perturbations: Causes and Consequences* (Vol. 424, p. 0). Geological Society of America. https://doi.org/10.1130/2007.2424(01)

Thomas, E., Boscolo-Galazzo, F., Balestra, B., Monechi, S., Donner, B., & Röhl, U. (2018). Early Eocene Thermal Maximum 3: Biotic Response at Walvis Ridge (SE Atlantic Ocean). *Paleoceanography and Paleoclimatology*, *33*(8), 862–883. https://doi.org/10.1029/2018PA003375

Thomas, E., & Shackleton, N. J. (1996). The Paleocene-Eocene benthic foraminiferal extinction and stable isotope anomalies. *Geological Society, London, Special Publications*, *101*(1), 401–441. https://doi.org/10.1144/GSL.SP.1996.101.01.20

Tierney, J. E., Zhu, J., Li, M., Ridgwell, A., Hakim, G. J., Poulsen, C. J., Whiteford, R. D. M., Rae, J. W. B., & Kump, L. R. (2022). Spatial patterns of climate change across the Paleocene–Eocene Thermal Maximum. *Proceedings of the National Academy of Sciences of the United States of America*, *119*(42), e2205326119. https://doi.org/10.1073/pnas.2205326119

Torfstein, A., Winckler, G., & Tripati, A. (2010). Productivity feedback did not terminate the Paleocene-Eocene Thermal Maximum (PETM). *Climate of the Past*, *6*(2), 265–272. https://doi.org/10.5194/cp-6-265-2010

Tripati, A., & Elderfield, H. (2005). Deep-Sea Temperature and Circulation Changes at the Paleocene-Eocene Thermal Maximum. *Science*, *308*(5730), 1894–1898. https://doi.org/10.1126/science.1109202

Vaes, B., van Hinsbergen, D. J. J., van de Lagemaat, S. H. A., van der Wiel, E., Lom, N., Advokaat, E. L., Boschman, L. M., Gallo, L. C., Greve, A., Guilmette, C., Li, S., Lippert, P. C., Montheil, L., Qayyum, A., & Langereis, C. G. (2023). A global apparent polar wander path for the last 320 Ma calculated from site-level paleomagnetic data. *Earth-Science Reviews*, *245*, 104547. https://doi.org/10.1016/j.earscirev.2023.104547

Widlansky, S. J., Secord, R., Snell, K. E., Chew, A. E., & Clyde, W. C. (2022). Terrestrial carbon isotope stratigraphy and mammal turnover during post-PETM hyperthermals in the Bighorn Basin, Wyoming, USA. *Climate of the Past*, *18*(4), 681–712. https://doi.org/10.5194/cp-18-681-2022

Wieczorek, R., Fantle, M. S., Kump, L. R., & Ravizza, G. (2013). Geochemical evidence for volcanic activity prior to and enhanced terrestrial weathering during the Paleocene Eocene Thermal Maximum. *Geochimica et Cosmochimica Acta*, *119*, 391–410. https://doi.org/10.1016/j.gca.2013.06.005

Wing, S. L., Harrington, G. J., Smith, F. A., Bloch, J. I., Boyer, D. M., & Freeman, K. H. (2005). Transient Floral Change and Rapid Global Warming at the Paleocene-Eocene Boundary. *Science*, *310*(5750), 993–996. https://doi.org/10.1126/science.1116913

Winguth, A. M. E., Thomas, E., & Winguth, C. (2012). Global decline in ocean ventilation, oxygenation, and productivity during the Paleocene-Eocene Thermal Maximum: Implications for the benthic extinction. *Geology*, *40*(3), 263–266. https://doi.org/10.1130/G32529.1

Zachos, J. C., Pagani, M., Sloan, L., Thomas, E., & Billups, K. (2001). Trends, Rhythms, and Aberrations in Global Climate 65 Ma to Present. *Science*, *292*(5517), 686–693. https://doi.org/10.1126/science.1059412

Zachos, J. C., Röhl, U., Schellenberg, S. A., Sluijs, A., Hodell, D. A., Kelly, D. C., Thomas, E., Nicolo, M., Raffi, I., Lourens, L. J., McCarren, H., & Kroon, D. (2005a). Rapid Acidification of the Ocean During the Paleocene-Eocene Thermal Maximum. *Science*, *308*(5728), 1611–1615. https://doi.org/10.1126/science.1109004

Zachos, J. C., Röhl, U., Schellenberg, S. A., Sluijs, A., Hodell, D. A., Kelly, D. C., Thomas, E., Nicolo, M., Raffi, I., Lourens, L. J., McCarren, H., & Kroon, D. (2005b). Rapid Acidification of the Ocean During the Paleocene-Eocene Thermal Maximum. *Science*, *308*(5728), 1611–1615. https://doi.org/10.1126/science.1109004

Zachos, J. C., Schouten, S., Bohaty, S., Quattlebaum, T., Sluijs, A., Brinkhuis, H., Gibbs, S. J., & Bralower, T. J. (2006). Extreme warming of mid-latitude coastal ocean during the Paleocene-Eocene Thermal Maximum: Inferences from TEX86 and isotope data. *Geology*, *34*(9), 737–740. https://doi.org/10.1130/G22522.1

Zachos, J. C., Wara, M. W., Bohaty, S., Delaney, M. L., Petrizzo, M. R., Brill, A., Bralower, T. J., & Premoli-Silva, I. (2003). A Transient Rise in Tropical Sea Surface Temperature During the Paleocene-Eocene Thermal Maximum. *Science*, *302*(5650), 1551–1554. https://doi.org/10.1126/science.1090110

Zeebe, R. E., Bijma, J., & Wolf-Gladrow, D. A. (1999). A diffusion-reaction model of carbon isotope fractionation in foraminifera. *Marine Chemistry*, *64*(3), 199–227. https://doi.org/10.1016/S0304-4203(98)00075-9

Zeebe, R. E., & Lourens, L. J. (2019). Solar System chaos and the Paleocene–Eocene boundary age constrained by geology and astronomy. *Science*, *365*(6456), 926–929. https://doi.org/10.1126/science.aax0612

Zeebe, R. E., Ridgwell, A., & Zachos, J. C. (2016). Anthropogenic carbon release rate unprecedented during the past 66 million years. *Nature Geoscience*, *9*(4), Article 4. https://doi.org/10.1038/ngeo2681

Zeebe, R. E., & Zachos, J. C. (2007). Reversed deep-sea carbonate ion basin gradient during Paleocene-Eocene thermal maximum. *Paleoceanography*, *22*(3). https://doi.org/10.1029/2006PA001395

Zeebe, R. E., Zachos, J. C., & Dickens, G. R. (2009a). Carbon dioxide forcing alone insufficient to explain Palaeocene–Eocene Thermal Maximum warming. *Nature Geoscience*, *2*(8), Article 8. https://doi.org/10.1038/ngeo578

Zeebe, R. E., Zachos, J. C., & Dickens, G. R. (2009b). Carbon dioxide forcing alone insufficient to explain Palaeocene–Eocene Thermal Maximum warming. *Nature Geoscience*, *2*(8), Article 8. https://doi.org/10.1038/ngeo578

Zhang, J., Gilbert, D., Gooday, A. J., Levin, L., Naqvi, S. W. A., Middelburg, J. J., Scranton, M., Ekau, W., Peña, A., Dewitte, B., Oguz, T., Monteiro, P. M. S., Urban, E., Rabalais, N. N., Ittekkot, V., Kemp, W. M., Ulloa, O., Elmgren, R., Escobar-Briones, E., & Van der Plas, A. K. (2010). Natural and human-induced hypoxia and consequences for coastal areas: Synthesis and future development. *Biogeosciences*, *7*(5), 1443–1467. https://doi.org/10.5194/bg-7-1443-2010